

A Cyclone Phase Space Derived from Thermal Wind and Thermal Asymmetry

ROBERT E. HART

Department of Meteorology, The Pennsylvania State University, University Park, Pennsylvania

(Manuscript received 27 June 2001, in final form 5 August 2002)

ABSTRACT

An objectively defined three-dimensional cyclone phase space is proposed and explored. Cyclone phase is described using the parameters of storm-motion-relative thickness asymmetry (symmetric/nonfrontal versus asymmetric/frontal) and vertical derivative of horizontal height gradient (cold- versus warm-core structure via the thermal wind relationship). A cyclone's life cycle can be analyzed within this phase space, providing substantial insight into the cyclone structural evolution. An objective classification of cyclone phase is possible, unifying the basic structural description of tropical, extratropical, and hybrid cyclones into a continuum.

Stereotypical symmetric warm-core (tropical cyclone) and asymmetric cold-core (extratropical cyclone) life cycles are illustrated using 1° Navy Operational Global Atmospheric Prediction System (NOGAPS) operational analyses and 2.5° NCEP–NCAR reanalyses. The transitions between cyclone phases are clearly illustrated within the phase space, including extratropical transition, subtropical and tropical transition, and the development of warm seclusions within extratropical cyclones. The planet's northwestern hemisphere inhabitation of the proposed phase space between 1980 and 1999 is examined using NCEP–NCAR 2.5° reanalyses. Despite the inability to adequately resolve tropical cyclones at the coarse 2.5° resolution, warm-core cyclones (primarily warm-seclusion extratropical cyclones) have a mean intensity that is 10 hPa lower than that of cold-core cyclones. Warm-core cyclones also have a much larger variability for intensity distribution, with an increased occurrence of lower MSLP. Further, at 2.5° resolution the lowest analyzed MSLP for a warm-core cyclone was 14 hPa lower than that for a cyclone that remains cold core. These results suggest that cyclones that maintain solely a cold-core structure (no warm-seclusion or tropical development) may be associated with a significantly weaker minimum observed intensity at 2.5° resolution, although further examination using higher-resolution data is required to refine this.

Phase diagrams are being produced in real time to improve the forecasting of cyclone phase evolution and phase transitions, and to provide measures of phase predictability through ensembling of multiple models. The likelihood of warm-core development in cyclones can be anticipated by applying the diagnostics to various model forecasts, illuminating the potential for large intensity changes when the explicit model intensity forecasts may be insufficient.

1. Introduction

The formation, development, maturity, and decay of cyclones have been studied for decades, and through the 1950s it was generally believed that tropical cyclones had a life cycle that was distinct from extratropical cyclones. Tropical cyclones formed over warm water, intensified from wind-driven evaporation and the resulting latent heat release, and decayed over colder water or land (Charney and Eliassen 1964). Extratropical cyclones formed within the middle latitudes, largely as a consequence of the temperature gradients and wind shear intrinsic to those latitudes, and then decayed as the instability was removed with occlusion (Bjerknes and Solberg 1922; Charney 1947; Eady 1949). There were two seemingly well-defined types of cyclones with

little acknowledgment of a gray area between them, largely due to the lack of high-resolution satellite or maritime observations.

This discrete separation between cyclone types would gradually break down over the subsequent decades as landfalling hurricanes and satellite imagery provided increased observations of more varied cyclone structure and evolution. Tannehill (1938) and Pierce (1939) documented the formation of frontal structure with the great New England hurricane of 1938 as it made landfall. Further observation of landfalling tropical cyclones in the 1950s–1970s found similar frontal structure and evolution away from a tropical structure within previously tropical cyclones (Knox 1955; Sekioka 1956a,b, 1957; Palmén 1958; Kornegay and Vincent 1976; Brand and Guard 1978). These works illustrated that the transition between cyclone types was a gradual process, with the potential for a hybrid phase between them that was not previously acknowledged.

Evidence for cyclones that have partial characteristics

Corresponding author address: Robert E. Hart, Dept. of Meteorology, The Pennsylvania State University, 503 Walker Bldg., University Park, PA 16802.
E-mail: hart@ems.psu.edu

of tropical cyclones (subtropical cyclones) was documented, including guidelines for diagnosing structural changes and intensity from satellite imagery (Hebert and Poteat 1975). These cyclones typically have only a weak lower-tropospheric warm-core structure resulting from the lack of sustained convection near the cyclone center. The displacement of convection from the cyclone center often results from weak frontal structure within the subtropical cyclone, forcing mesoscale ascent away from the core. A large radius of maximum winds is associated with these cyclones, which is more typical of a weak extratropical cyclone than a tropical cyclone. The conversion of a subtropical cyclone into a full tropical cyclone requires the development and maintenance of convection near the cyclone core. This conversion can be diagnosed using satellite imagery, but is often quite difficult to forecast since the evolution within numerical models is so subtle and poorly indicated using conventional analyses. Further, the development of tropical cyclones from weak extratropical cyclones was also noted with the advent of satellite imagery, although such development is unusual given the synoptic pattern required to introduce an extratropical cyclone over sufficiently warm sea surface temperatures and low wind shear. Understanding and diagnosing these unconventional modes of warm-core development are significant beyond the simple need for objective classification. The development of a full-tropospheric warm core implies that the potential cyclone intensity change and its predictability have become, in the mean, significantly more complex and larger amplitude than was the case prior to warm-core transition.

In the subsequent decade, it was found that the processes known to be critical for tropical cyclone development could also have a major influence on extratropical cyclone development. The crucial role of surface fluxes and convection in coastal baroclinic cyclogenesis was illustrated (Bosart 1981). Not only did this study diagnose one major limitation preventing successful numerical forecasts of explosive cyclogenesis at the time, but it illustrated that mesoscale changes can significantly impact synoptic-scale cyclone evolution. Soon after, the sensitivity of extratropical development to the magnitude and vertical distribution of convective heating was also explored (Gyakum 1983a,b), illustrating strong sensitivity of modeling baroclinic cyclogenesis to the convective scale. The strong role the subgrid scale can play in extratropical cyclone development would be realized as higher-resolution models with more sophisticated physics drove an increase in the forecast accuracy of explosive cyclogenesis in the 1980s (Sanders 1987). The strong impact of oceanic surface fluxes, convection, and convective heating on extratropical cyclones suggested that warm-core development within extratropical cyclones might indeed be possible in extreme circumstances. Later research in the 1990s would show that warm-core development in extratropical cyclones can result over land, when explosive baroclinic development leads

to a trapped region of warm air near the cyclone center (warm seclusion).

The increasing availability of higher-resolution satellite data and surface observations sparked considerable research into the processes that generated such unconventional cyclones. These intense higher-latitude cyclones often defied the conventional definition for extratropical cyclone development and structure (Bjerknes and Solberg 1922). Significant convection, a contraction of the cyclone wind field, a temperature maximum near the cyclone center, and a lower-tropospheric vorticity maximum were observed (Bosart 1981; Gyakum 1983a,b; Kuo et al. 1992). Shapiro and Keyser (1990) have since proposed an extension to the conventional Norwegian cyclone model (Bjerknes and Solberg 1922), where the warm-seclusion process was described for intense extratropical cyclones. The development of the warm-seclusion phase of an extratropical cyclone could be produced through purely adiabatic processes (Reed et al. 1994) although earlier studies (Gyakum 1983a,b; Kuo et al. 1992) showed that diabatic effects could enhance the adiabatically driven warm-seclusion development.

In the 1980s and 1990s research into extratropical transition of tropical cyclones underwent a rebirth. Extratropical transition, at its most extreme, was found to be the introduction of a deep warm-core cyclone just downstream of a deep cold-core trough or preexisting extratropical cyclone (DiMego and Bosart 1982a,b; Harr and Elsberry 2000; Harr et al. 2000; Klein et al. 2000; Hart 2001). This fortuitous convergence of both conventional cyclone types is only feasible for a few months per year in the North Atlantic (Hart and Evans 2001), and is most frequently observed in the western Pacific and North Atlantic basins. Often, the resulting transitioned cyclone retains characteristics of both parent systems. The maintenance of a partial warm-core structure of previously tropical cyclones well into the middle latitudes (Thorncroft and Jones 2000; Hart 2001) blurs the distinction between a transitioning tropical cyclone and a warm-secluded extratropical cyclone (Hart 2001). Further, evidence of warm-core formation and development in unconventional environments was shown by Bosart and Bartlo (1991), Bosart and Lackmann (1995), Beven (1997), and Miner et al. (2000). Yet, Atlantic tropical cyclones that underwent the most spectacular cases of extratropical transition and post-transition intensification were those that formed in the (conventional) Tropics south of 20°N (Hart and Evans 2001). Thus, the warm-core cyclones that intensify the most after extratropical transition are those that, on average, attain the strongest warm-core structure prior to transition. The cyclone's future structure and intensity are determined, in part, by the cyclone's history back as far as its formation location.

The previously sharp boundary distinguishing tropical cyclones from extratropical cyclones in the first half of the twentieth century has been substantially weak-

ened. As a result of the numerous examples of unconventional cyclone structure and development, the meteorological community is now attempting to use a more flexible approach toward classification of the three-dimensional nature of cyclone structure (referred to here as cyclone phase). However, an objective, consistent approach has not yet been agreed upon. At the beginning of the twenty-first century the community has progressed toward an understanding of cyclone variability that suggests the cyclone phase space is not a mutually exclusive set of cyclone types, but rather a broad continuum. At one end of this continuum lies the conventional extratropical cyclone; at the other end lies the conventional tropical cyclone. The vast majority of cyclones we observe, however, seem to lie within the interior of this continuum (Beven 1997; Reale and Atlas 2001). Beven (1997) appears to be the first to suggest a phase space for cyclones, defining them by two parameters: core temperature (warm to cold) and frontal nature. The Beven (1997) phase diagram was a substantial step forward, and provided motivation to pursue a more rigorous definition and analysis of cyclone phase.

Currently, a consistent, objective method for diagnosing the cold- versus warm-core structure within cyclones has not been agreed upon, and examinations of conventional model fields do not provide for a diagnosis of cyclone phase. Although detailed examination of conventional meteorological fields (wind, vorticity, potential vorticity, equivalent potential temperature, Q vectors) provides great insight into the cyclone structure, those same fields are not adequate for uniquely determining the phase of the cyclone, and whether models are indicating a trend in that phase. Indeed, it is often difficult to distinguish tropical cyclone development from subtropical cyclone development or hybrid cyclone development, especially outside the Tropics, within operational forecast models. Yet, knowledge of the nature of the forecast cyclone's development within those models is essential to quantifying the potential threat and intrinsic intensity forecast uncertainty associated with that cyclone. It can be significantly more valuable to know that a model-forecast subtropical cyclone has become deep-tropospheric warm core (the model's representation of a conversion to a tropical cyclone), for example, than the actual intensity as forecast by the model. Thus, for both the extratropical cyclone and tropical cyclone communities, diagnostics indicating cyclone phase would be helpful for understanding the current and forecast cyclone evolution and threat given by numerical models.

An objectively defined phase diagram for characterizing the phase and structure of cyclones is proposed here. Any cyclone that has a well-resolved three-dimensional height field can be objectively analyzed within the proposed phase space. Construction and interpretation of the phase diagram are described (section 2) and examples using conventional tropical cyclone and extratropical cyclone cases are presented (section 3).

Less frequently occurring modes of cyclone development (extratropical transition, tropical transition, and warm seclusion) are explored (section 4) and a 20-yr examination of the phase space climatology is examined (section 5). Finally, the potential application of this research to operational forecasting of cyclone evolution and predictability is shown (section 6), followed by a concluding summary (section 7).

2. Methodology

The definitions and method behind cyclone detection are tracking, the construction of the proposed phase diagram, and the datasets used are presented below.

a. Definitions

1) CYCLONE DETECTION AND TRACKING

For the case examples shown in sections 3 and 4, cyclone tracking was done manually using MSLP minima. However, for the 20-yr phase climatology in section 5 and the real-time forecast Web page application described in section 6, an automated procedure for cyclone tracking is necessary. This detection and tracking procedure utilizes the approaches of Zishka and Smith (1980), Williamson (1981), Harr et al. (1983), and Marchok (2002), although with considerable less complexity than the latter approaches. While it is beyond the scope of this research to produce an optimal tracking routine, a reliable one is needed to produce an accurate phase climatology (section 5) and automated operational forecast phase diagrams (section 6).

(i) Cyclone detection

A cyclone is defined here using the following criteria: 1) a local minimum of sea level pressure (MSLP) less than 1020 hPa within the interior of a 5° box, 2) a lifespan of at least 24 h, and 3) an MSLP gradient of 2 hPa within the 5° box. At each time period within the gridded analysis or forecast, a cyclone was found if the minimum MSLP within the $5^\circ \times 5^\circ$ box was not located on the edges of that box (criterion 1). This $5^\circ \times 5^\circ$ "search" box was then moved across the domain, partially overlapping the previous box location to ensure detection of cyclones that fall on the box edge. The size of the search box chosen determines the scale of the cyclones that are found. If all mesoscale low pressure systems are desired as well, a smaller search box would need to be used (and perhaps a smaller lifespan criteria). The 24-h lifespan (criterion 2) is used to exclude spurious MSLP minima and is comparable to that used in Zishka and Smith (1980), but less than the 36-h criterion used by Harr et al. (1983). As higher-resolution data and further computer resources become available, a smaller box size may be tested so that all mesoscale cyclones may be tracked as well. The MSLP gradient condition (criterion 3) is needed to avoid locating nu-

TABLE 1. Thresholds of cyclone direction change for cyclone tracking.

Cyclone speed between two consecutive analysis or forecast times (m s^{-1})	Corresponding maximum allowed change in cyclone direction of motion ($^{\circ}$)	Relative shape and size of cyclone track search area	Applicable grid resolution ranges for 6-h increment ($^{\circ}$)
<10	No restriction	Small circle	All
10	135	$\frac{3}{4}$ of a circle	≤ 1.0
15	90	Larger semicircle	≤ 1.0
20	75	Broad cone	≤ 2.5
25	60	Long cone	≤ 2.5
≥ 30	45	Long, narrow cone	≤ 2.5

merous weak minima in MSLP within the Tropics when the overall pressure field is generally uniform and is comparable to that used by NCEP for tracking tropical cyclones [$1 \text{ hPa } 333 \text{ km}^{-1}$; Marchok (2002)].

(ii) Cyclone tracking

All cyclones are assumed to be newly formed, unless stringent criteria for cyclone tracking are satisfied. These criteria essentially define the size and shape of the “search area” for cyclone movement, and are qualitatively similar to those derived by Williamson (1981) and later implemented at the Navy Research Laboratory (NRL) (Harr et al. 1983, 1992). Sea level pressure minima at two consecutive analysis or forecast times (cyclone A at time $t - \Delta t$ and cyclone B at time t) separated by a distance Δd are deemed to be the *same* cyclone at those two consecutive times only if the following tracking criteria are met:

- 1) $\Delta t \leq 24 \text{ h}$;
- 2) cyclone B is the closest cyclone at time t to where cyclone A was at time $t - \Delta t$;
- 3) V (implied movement of the cyclone) = $\Delta d / \Delta t < 40 \text{ m s}^{-1}$;
- 4) $\Delta d < \Delta d_{\text{MAX}}$ (maximum allowed movement over Δt), where

$$\Delta d_{\text{MAX}} = \text{Max}(500\text{km}, 3 \times \Delta t \times V_{\text{PREV}}); \text{ and } (1)$$
- 5) the cyclone direction of motion change from $t - 2\Delta t \rightarrow t - \Delta t$ to $t \rightarrow t - \Delta t$ is within a limited angular range, where this range is a function of the cyclone’s implied speed, V (Table 1).

Here, V_{PREV} is the previous speed of cyclone A (between $t - 2\Delta t$ and $t - \Delta t$). Conditions 2 and the 500-km minimum threshold of condition 4 allow for easy tracking of slow-moving cyclones. Conditions 3–5 are based upon an analysis of 115 yr of North Atlantic cyclone climatology using the National Hurricane Center’s (NHC) best-track database (Jarvinen et al. 1984; Neumann et al. 1993). This database includes all stages of tropical cyclone development, including extratropical. For tracking of fast-moving cyclones, the cyclone is allowed to move more than 500 km over Δt if the resulting speed (V) is (condition 3) less than 40 m s^{-1} and (condition 4) not more than triple the speed during

the previous time period (V_{PREV}). This latter condition, which defines the size of the tracking search area, is based on the result (not shown) that if the speed increases by more than a factor of 3 over a distance of greater than 500 km, the two cyclones are not the same, or too long a period of time has passed (from missing data) to ensure reliable tracking. Only one 6-h analysis time in 115 yr of data violated this condition. The 40 m s^{-1} maximum implied speed in condition 3 is based upon the upper limit of 6-h cyclone speed in this 115-yr analysis (Fig. 1). Given the broader seasonal application of this tracking procedure, this speed threshold is necessarily higher than that used by the National Centers for Environmental Prediction (NCEP) for purely hurricane tracking [30 m s^{-1} ; Marchok (2002)].

The fifth condition (Fig. 1 and resulting Table 1) defines the shape of the tracking search area and is critical to avoid erroneous retrograding or discontinuous jumps in cyclone tracking (Williamson 1981; Harr et al. 1983). A slow-moving cyclone is allowed to change its direction the maximum of 180° , while a fast-moving cyclone has a narrow range of possible motion vectors determined by the previous motion of the cyclone. Criteria 4 and 5 result in a smaller-radius circular search area for slowly moving cyclones. At higher translation speeds, this search area becomes increasingly narrow and cone shaped, but also of larger radius.

It is important to note that the constraints in Table 1 must be consistent with the resolution of the gridded data, allowing for a diagonal one-gridpoint backward move over 6 or 12 h. For 2.5° resolution data, a diagonal one-gridpoint move over 6 h represents a maximum speed of 18.2 m s^{-1} . Thus, the lowest applicable threshold in Table 1 for 2.5° data is 20 m s^{-1} (hence the open circles in Fig. 1). For higher-resolution data at 6-h resolution (Table 2), the 10 and 15 m s^{-1} thresholds are permissible.

(iii) Differences from other tracking algorithms

For computational efficiency in cyclone detection and tracking of a large number of cyclones for many models (e.g., section 6), the approach just described necessarily must be less complex than more complete cyclone trackers. Harr et al. (1983, 1992), and Marchok (2002) use a Barnes analysis or regression to interpolate between-

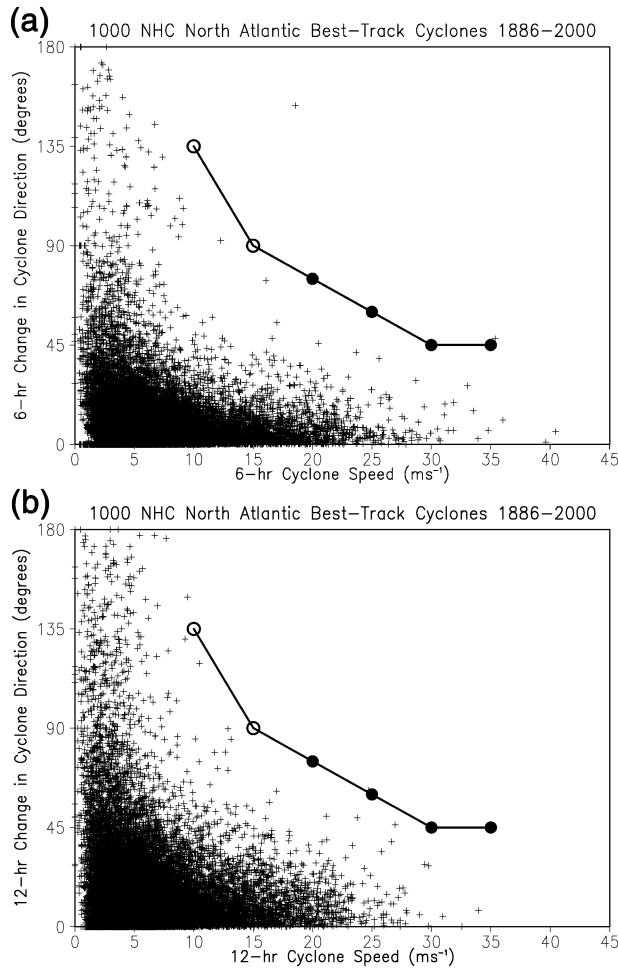


FIG. 1. The (a) 6- and (b) 12-h cyclone change in direction of motion as a function of translation speed ($m s^{-1}$) using 1000 tropical cyclones from the 1886–2000 NHC best-track dataset (Jarvinen et al. 1984; Neumann et al. 1993). All tropical cyclone phases are included (tropical depression to extratropical). This analysis was used to arrive at thresholds for maximum allowable change in direction of motion necessary for reliable automated cyclone tracking. The circles are those thresholds used for cyclone tracking in the climatology in section 5, as well as on the Web site described in section 6. The open circles at 10 and 15 $m s^{-1}$ indicate that that threshold is used only when the grid resolution is sufficiently high ($\leq 1^\circ$). See also Table 1.

model grid points to locate cyclone position. In the algorithm used here, a cyclone center will always fall on a model grid point. Further, this approach uses only MSLP whereas Marchok (2002) synthesizes MSLP and vorticity at 850 and 700 hPa to arrive at a consensus cyclone location. Sinclair (1994) has shown the limitations and benefits of using either MSLP or vorticity for tracking. During the formative stages of midlatitude cyclone development, a closed vorticity contour is more indicative of the cyclone center than a closed MSLP contour. Additionally, vorticity is able to diagnose weak, lower-latitude cyclones (tropical depressions, for example) more frequently than MSLP. However, the synthesis of MSLP and vorticity in tracking tropical cyclones is more easily accomplished since those cyclones are nearly vertically stacked and, at 1° – 2.5° resolution, the vorticity maximum is nearly collocated with the MSLP minima. For developing extratropical cyclones, the region of maximum vorticity may be located a significant distance from the area of lowest pressure (especially at 700 hPa upward). This presents the problem of resolving two estimates of cyclone location displaced by a significant distance.

As a result of these complexities, and when considering the resolution of data used here and the goal of tracking both tropical and extratropical cyclones, the use of MSLP for cyclone tracking is a reasonable compromise, acknowledging the limitations discussed above, and in more detail below. For the selection of cases shown in sections 3 and 4, the cyclone center position was adjusted randomly by 50–100 km and the phase analyses were recalculated (not shown). There was no dramatic change, either qualitatively or quantitatively, in the phase diagnosis of the cyclones.

(iv) Tracking climatology and known tracking errors

The qualitative distribution of cyclone climatology produced by the tracking algorithm using 20 yr of NCEP–National Center For Atmospheric Research (NCAR) reanalysis data (Kalnay et al. 1996 and section 5) was compared (not shown) to previous manual cyclone climatologies (e.g., Zishka and Smith 1980). In particular, the maxima of cyclone activity over northern Texas, the Great Lakes to Hudson Bay, and offshore of the U.S. northeast coast to the Canadian Maritimes were well re-

TABLE 2. Datasets.

Dataset	Horizontal resolution ($^\circ$)	Vertical resolution (no. of levels)	Period used	Use of TC bogus in analysis/initial conditions
NCEP reanalysis	2.5°	17	1986–99	No TC bogus
ECMWF reanalysis	1.125°	30	1979–93, Jul–Nov	No TC bogus
NOGAPS analysis	1°	16	1998–2000, Jun–Dec	TC bogus 1998–2000
AVN forecast	1°	26	2001	No TC bogus 2001
CMC forecast	1°	26	2001	TC bogus 2001
NOGAPS forecast	1°	16	2001	TC bogus 2001
UKMET forecast	1.25°	10	2001	TC bogus 2001

produced. However, several small areas of high cyclone activity were falsely produced by the algorithm. The tracking procedure tends to detect quasi-stationary areas of lower pressure that are climatological or seasonal rather than of a synoptic-scale, transient nature. The calculation of MSLP over regions of high terrain in the summer can lead to nonphysical areas of significantly lower MSLP (resulting from extrapolation well below ground from an elevated heat source in the calculation of MSLP), such as over northwest South America, Central America, the Rocky Mountains, and parts of interior Greenland. Additionally, there are two regions of climatological quasi-stationary lower pressure that will frequently be misidentified as a cyclone: over the Mojave Desert in the southwestern United States and northern Africa. The use of MSLP (rather than vorticity) as the background field for cyclone detection leads to these five areas of falsely diagnosed cyclone locations. The impact of these falsely diagnosed events on the 20-yr phase climatology is discussed in section 5.

There are additional limitations using this detection and tracking method, most notably for the formation of two cyclones in close proximity. In this case, the tracking routine may either jump to the other cyclone (leading to the track discontinuity), or be unable to diagnose one of the two cyclones if they both fall within the $5^\circ \times 5^\circ$ box described earlier, and are slow moving. As model resolution improves and computer resources increase, the ability to use a smaller tracking box that will detect a larger percentage of cyclones will be possible. In practice, the cyclone tracker has been successful at distinguishing two cyclones that are sufficiently close for binary (Fujiwhara) interaction, such as western North Pacific Typhoons Fengshen and Fung-wong in 2002, which came within 600 km of one another at their closest approach (not shown). When the phase space is used in a real-time forecast setting (section 6), it is expected that the user will, through the use of conventional tools, be aware of instances when the tracker is having difficulty distinguishing two cyclones in close proximity. In these cases, the resulting phase diagrams may be in question.

2) CYCLONE STRUCTURE: PHASE PARAMETERS

A successful phase space would require parameters that simultaneously describe the strength of the warm-core structure within a tropical cyclone and the cold-core structure within an extratropical cyclone, while also describing the stage of cold-core extratropical development (formation, intensification, occlusion, and decay). Accordingly, the parameters would have to account for the vertically stacked nature of the tropical cyclone and the tilted nature of the extratropical cyclone. The parameters would have to diagnose the transitions in cyclone phase, such as the extratropical transition of a tropical cyclone, the transition of a subtropical cyclone into a warm-core tropical cyclone, and the development

of warm seclusion in extratropical cyclones. Many parameters were examined, based on potential vorticity and its vertical profile, Q vectors, equivalent potential temperature and its vertical profile, frontogenesis, and cyclone tilt, to name a few. After careful examination of these more complex parameters, it was found that two simpler, yet fundamental, measures of cyclone structure were the most robust: thermal wind and thermal asymmetry, as discussed below.

The three parameters used to describe the general structure of cyclones are the lower-tropospheric thermal asymmetry (parameter B), the lower-tropospheric thermal wind (cold versus warm core, parameter $-V_7^{\theta}$) and the upper-tropospheric thermal wind (cold versus warm core, parameter $-V_7^{\theta}$). These three parameters are successful at succinctly describing and differentiating the structure of tropical and extratropical cyclones (sections 3 and 4), a task that other parameters (when reduced to scalar values necessary for a phase space) could not easily achieve on their own. While many parameters of cyclone structure (e.g., potential vorticity, conveyor belts, secondary circulations, jet streak configuration, cyclone tilt) are exceptional at describing the various aspects of cyclone evolution, their complex distribution within a cyclone is not easily utilized to create a practical and robust phase diagram. The three chosen parameters are simply calculated solely from the three-dimensional height field and have strong physical foundations with cyclone development theories, as we understand them.

While the three chosen parameters successfully summarize one cyclone phase space, a complete description of the cyclone structure requires the synthesis of the model diagnostics described here with conventional fields and direct observations from surface stations, rawinsondes, and satellite imagery. The actual complete cyclone phase space must have far more than three dimensions, and it should not be expected that every aspect of cyclone structure or development can be captured by the three chosen here.

(i) Parameter B: Cyclone thermal symmetry

The distribution of cyclones in the world can first be split into roughly two idealized classes: those that derive some fraction of their development from the horizontal temperature gradients (asymmetric or frontal; e.g., extratropical cyclone) and those that do not (symmetric or nonfrontal; e.g., tropical cyclone). Further, it is well established that the strength of the temperature gradients in the former group varies with time, depending on the stage of cyclone development (developing, mature, occlusion). The frontal nature of the cyclone (or lack thereof) and its sign are fundamental indicators of the type of cyclone and the stage of evolution. This frontal nature is defined here as the storm-motion-relative 900–600-hPa thickness asymmetry across the cyclone within 500-km radius, B:

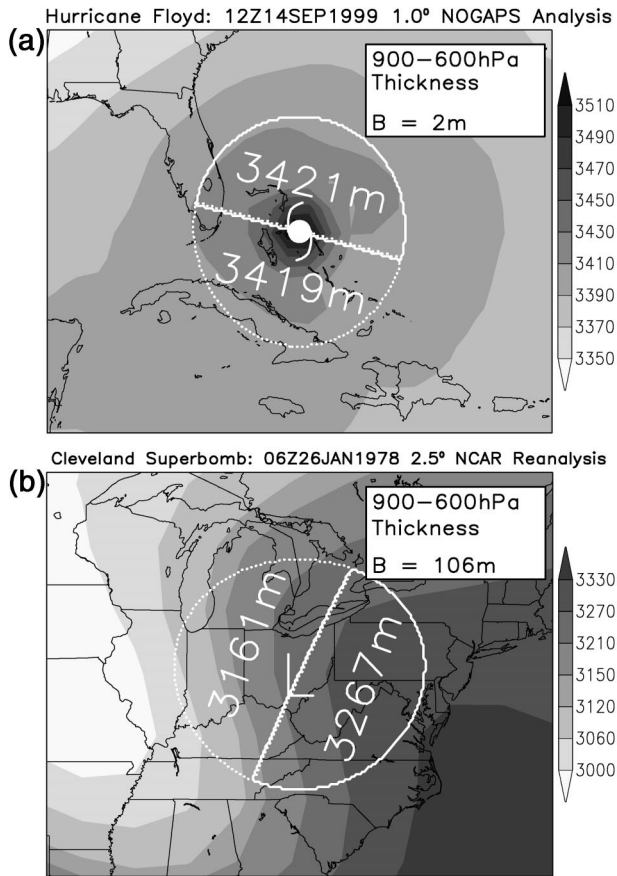


FIG. 2. Example 900–600-hPa thicknesses (shaded) across a (a) thermally symmetric (nonfrontal) tropical cyclone (Hurricane Floyd on 14 Sep 1999; 1° NOGAPS analysis) and (b) thermally asymmetric (frontal) extratropical cyclone [“Cleveland superbomb” on 26 Jan 1978; 2.5° NCEP–NCAR reanalysis; see also Hakim et al. (1995, 1996)]. Cyclone center is labeled within the 500-km-radius circle and the bisecting equator indicates direction of motion. The solid semicircle lies to the right of motion and dotted semicircle lies to the left of motion. The mean thickness for each semicircle is labeled, along with the difference between the semicircles, parameter B [Eq. (2)].

$$B = h(\overline{Z_{600 \text{ hPa}} - Z_{900 \text{ hPa}}}|_R - \overline{Z_{600 \text{ hPa}} - Z_{900 \text{ hPa}}}|_L), \quad (2)$$

where Z is isobaric height, R indicates right of current storm motion, L indicates left of storm motion, and the overbar indicates the areal mean over a semicircle of radius 500 km (Fig. 2). The integer h takes a value of +1 for the Northern Hemisphere and -1 for the Southern Hemisphere. All cases examined here are within the Northern Hemisphere, although a few Southern Hemisphere cases were examined for completeness (Evans and Hart 2003). The use of a layer average virtual temperature (thickness) in calculating B (instead of temperature on an isobaric surface) makes the parameter resistant to short-term fluctuations in temperature at any given pressure level that may result from transient convective activity. The pressure range used to calculate thickness was chosen to avoid the boundary layer and potential interpolation below ground. In regions where

the elevation is significantly higher than 900 hPa, the phase diagnostics must be used with caution since isobaric height fields extrapolated below ground will enter the calculation of B . The definition of B successfully distinguishes asymmetric frontal zones (Fig. 2b; see also Hakim et al. 1995, 1996) from symmetric local extrema of temperature associated with tropical cyclones (Fig. 2a). Thus, the parameter measures a gradient of mean-layer temperature perpendicular to the motion of the storm, and not simply the range of temperature across the cyclone circulation. This latter distinction becomes important for distinguishing thermally direct circulations from those that are thermally indirect, and aiding diagnosis of the extratropical cyclone life cycle.

A mature tropical cyclone has a value for B that is approximately zero (thermally symmetric or nonfrontal; Fig. 2a), while a developing extratropical cyclone has a large positive value for B (thermally asymmetric or frontal; Fig. 2b). A positive value of B indicates cold (warm) air left (right) of the cyclone track for the Northern (Southern) Hemisphere, consistent with the thermal wind relationship between temperature gradient and vertical shear of the horizontal wind. Quasigeostrophic theory (Sutcliffe 1947; Petterssen 1956; Trenberth 1978) dictates rising air downstream of storm motion (from positive vorticity advection increasing with height) and sinking air upstream of storm motion (from negative vorticity advection increasing with height). Since a positive value of B indicates warm advection downstream of the cyclone, it would also be associated with a thermally direct circulation when superimposed on the previously described synoptic-scale ascent field. Conversely, a negative value of B indicates cold advection downstream of the cyclone, and a thermally indirect circulation.

A convenient and physically sound threshold for distinguishing a tropical thermal gradient from a nontropical thermal gradient is $B = 10$ m (Hart 2001; Evans and Hart 2003). As examined through 1.125° European Centre for Medium-Range Weather Forecasts (ECMWF) reanalyses (Gibson et al. 1997), no major hurricane (winds of greater than 115 kt) had associated with it a value of B that exceeded 10 m (Hart 2001). As it is reasonable to argue that major hurricanes can sustain themselves only within a truly tropical environment, such a threshold of B for distinguishing a frontal from nonfrontal structure is sound. Accordingly, this 10-m threshold for B is used here to distinguish a nonfrontal cyclone from a marginally frontal cyclone. This 10-m threshold also provides for correct phase diagnosis of nonfrontal cyclones when the cyclone center does not lie exactly on a grid point (producing a value of B close to, but not exactly, 0 m; e.g. $B = 2$ m in Fig. 2a).

Within the range of 250–1000 km, the radius chosen to calculate B does not significantly impact the analysis of conventional tropical or extratropical cyclones. For this range of radius, the magnitude of B is always large for developing or mature extratropical cyclones and

nearly zero for tropical cyclones and occluded extratropical cyclones (not shown). While the magnitude of B changes slightly over this range of radius for conventional cyclones, the sign of B does not. The choice of radius for B does have a significant role, however, during phase transitions or cyclone interaction, for tropical cyclones in particular. Depending on the radius of examination, the magnitude or even sign of B can change significantly during the extratropical transition of a tropical cyclone, for example. An appropriate radius for B would be one that includes the convergent circulation of the tropical cyclone, but does not extend into other systems that are not yet influencing the tropical cyclone. Accordingly, the radius for B was chosen to be consistent with the average radius over which cyclonic, convergent inflow was observed for tropical cyclones: 4° – 6° (Frank 1977). This physical foundation of using a 500-km radius for B , in concert with the $B = 10$ m threshold for distinguishing symmetric from asymmetric cyclones, are borne out in its successful use for diagnosing the initiation of extratropical transition of tropical cyclones (Hart 2001; Evans and Hart 2003).

Since the radius chosen for calculating B is based upon the mean horizontal size of a distribution of 143 tropical cyclones (Frank 1977), there will be exceptions where the chosen radius is insufficient. For extremely small tropical cyclones, a radius smaller than 500 km may be necessary to accurately calculate the thermal symmetry of the tropical cyclone. While the convergent, cyclonic region of a tropical cyclone may vary by 100 km from the mean of approximately 500 km (Frank 1977), this variability is small compared to the resolution and accuracy of the gridded analyses. As higher-resolution global analyses become available, future research should examine a storm-size-dependent method for radius to more precisely define the cyclone phase than can be accomplished today.

(ii) Parameters $-V_T^L$ and $-V_T^U$: Cyclone thermal wind—Cold versus warm core

The determination of cold- versus warm-core vertical structure is the distinction of whether the magnitude of the cyclone isobaric height gradient (thus, geostrophic wind magnitude) above the surface cyclone center increases (cold core) or decreases (warm core) with height. This fundamental difference of thermal wind structure between tropical and extratropical cyclones was exploited to diagnose the cold- versus warm-core evolution of cyclones, and is the basis for the second and third cyclone parameters.

While all cyclones are both cold and warm core at the same time, depending on the atmospheric layer examined [Hirschberg and Fritsch (1993); see also stratosphere versus troposphere in Fig. 3], the focus in this paper is on the tropospheric phase. Warm-cold core distinction is made here based upon the examination of two tropospheric layers of equal mass: 900–600 hPa

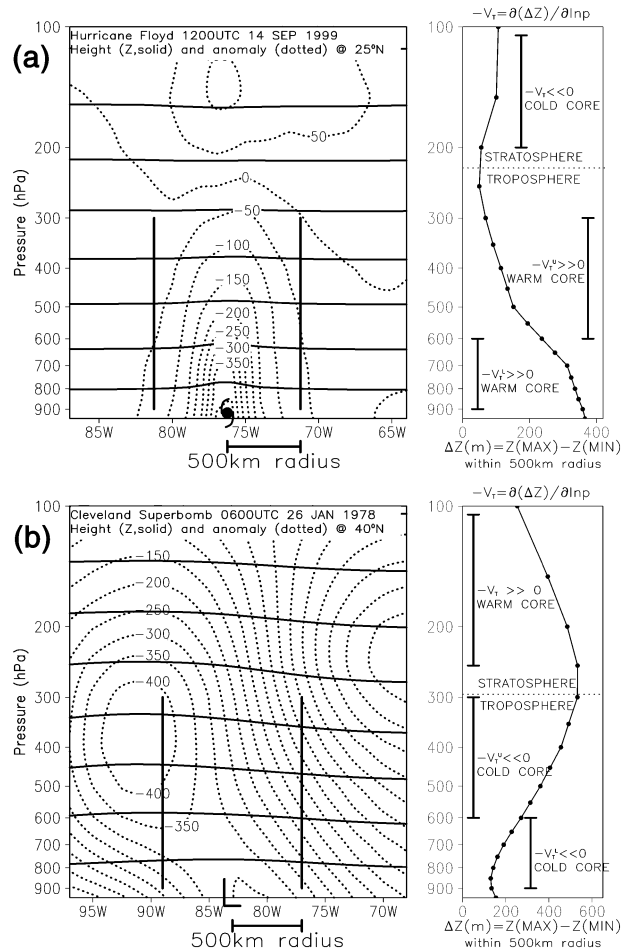


FIG. 3. Derivation of parameters $-V_T^L$ [Eq. (5)] and $-V_T^U$ [Eq. (6)] for (a) TC exhibiting tropospheric warm-core structure (Hurricane Floyd on 14 Sep 1999; 1° NOGAPS analysis) and (b) extratropical cyclone exhibiting tropospheric cold-core structure (Cleveland superbomb on 26 Jan 1978; 2.5° NCEP–NCAR reanalysis). (left) Longitudinal cross section of height (Z , m; solid contour every 2000 m) and anomaly from zonal mean (dotted, m). Two vertical lines indicate the 500-km radius. (right) Height difference (ΔZ) within this radius. Cyclone phase is derived from thermal wind $[\partial(\Delta Z)/\partial \ln p]$ in two layers. $-V_T^L$ is calculated using a linear-regression fit of ΔZ between 900 and 600 hPa; $-V_T^U$ is calculated between 600 and 300 hPa. Anomaly from zonal mean (dotted on left) clearly illuminates cyclone tilt in (b). It is the tilt that leads to the correct cold-core diagnosis in (b).

[consistent with B , Eq. (2)] and 600–300 hPa. As was the case in the calculation of B [Eq. (2)], the atmosphere below 900 hPa is not included in the calculation to avoid extrapolation below ground or within the boundary layer, which is not always representative of the free-atmosphere cyclone structure. The atmosphere above 300 hPa was excluded to prevent frequent inclusion of the stratospheric phase, which is often the opposite of the tropospheric phase (Fig. 3).

Thus, the cyclone height perturbation (ΔZ),

$$\Delta Z = Z_{\text{MAX}} - Z_{\text{MIN}}, \quad (3)$$

is evaluated within a radius of 500 km (Fig. 3), consistent with the radius used for the calculation of B [Eq. (2)]. If we define d as the distance between the geopotential extrema in Eq. (3) and f as the Coriolis parameter, then ΔZ is proportional to the magnitude of the geostrophic wind (\mathbf{V}_g):

$$\Delta Z = dg|\mathbf{V}_g|/f. \quad (4)$$

Accordingly, Miner et al. (2000) show how the temporally changing vertical profile of geostrophic wind could be used to evaluate the structural evolution of a hybrid Great Lakes cyclone. The vertical structure of the cyclone (cold versus warm core) is then defined as the vertical derivative of ΔZ , which simplifies to a scaled thermal wind (V_T) magnitude for constant d , as applied to the two tropospheric layers of equal mass:

$$\left. \frac{\partial(\Delta Z)}{\partial \ln p} \right|_{900 \text{ hPa}}^{600 \text{ hPa}} = -|V_T^L| \quad \text{and} \quad (5)$$

$$\left. \frac{\partial(\Delta Z)}{\partial \ln p} \right|_{600 \text{ hPa}}^{300 \text{ hPa}} = -|V_T^U|. \quad (6)$$

A linear regression fit to the vertical profile of ΔZ in Eqs. (5) and (6) provides an unambiguous magnitude and sign for $-V_T$ even in nonlinear vertical profiles of height perturbation (Fig. 3). It is fundamentally the slope of the profile in the right half of Fig. 3 that is being calculated in Eqs. (5) and (6). An interpolating vertical increment of 50 hPa was used to more accurately calculate the vertical profile of ΔZ , giving seven pressure levels on which the linear regression was performed in Eqs. (5) and (6). Positive values of $-V_T$ indicate a warm-core cyclone within the layer, while negative values of $-V_T$ indicate a cold-core cyclone within the layer. For a warm-core tropical cyclone, $-V_T^L$ and $-V_T^U$ both are necessarily positive, with $-V_T^L$ having the greater magnitude (Fig. 3a). Conversely, for a cold-core extratropical cyclone, $-V_T^L$ and $-V_T^U$ are necessarily negative, with $-V_T^U$ having the greater magnitude (Fig. 3b). Hybrid, warm-seclusion, and transitioning cyclones may have a sign of $-V_T^L$ that is different from $-V_T^U$ (section 4).

The cold- versus warm-core structure as defined here relates directly to the vertical structure of the cyclone's height perturbation (amplitude). As defined in Eqs. (5) and (6), a cold-core structure indicates a wave or cyclone structure that has a larger amplitude at the top of the layer than the bottom. Conversely, a warm-core structure (which is usually vertically stacked, within the resolution of the analyses) indicates a cyclone height perturbation that is larger at the bottom of the layer than the top. This relationship between cyclone thermal structure and the profile of height perturbation results directly from the hypsometric relationship, and is discussed in further detail for cold-core cyclones in Hirschberg and Fritsch (1993).

A cyclone's phase, as described in Eqs. (5) and (6),

will change as the height profile of the cyclone evolves, from both temperature advection and geostrophic adjustment. A negative temperature anomaly placed near the tropopause (consistent with an increasing cold-core structure) is able to perturb the height field downward to great depth (Hirschberg and Fritsch 1993) due to the greatly decreased air density and corresponding increased Rossby penetration depth at those altitudes. Conversely, a positive temperature perturbation in the lower troposphere (consistent with a warm-core structure) will communicate its influence through a relatively shallow depth of the lower troposphere. The height tendency within the column above the surface cyclone, the resulting vertical profile of height perturbation ΔZ (Fig. 3), and thus, Eqs. (5) and (6), reveal a great deal about the internal forces that are altering the net cyclone structure and intensity.

A radius of 500 km is consistent with the radius chosen for B [Eq. (2)] and is necessary to adequately resolve the vertical profile of horizontal height gradient produced from the natural tilt associated with extratropical cyclones through the troposphere (Fig. 3b). A tilted cyclone (usually westward tilt from baroclinic theory) increases the cold-core profile, as shown in Fig. 3b. Through this tilt the wave amplitude and, therefore, ΔZ increases significantly with height. Therefore, although a radius of 500 km may not completely resolve the axis of the tilted height minima (dotted in Fig. 3b.), the cold-core thermal wind structure is still correctly evaluated within the 500-km radius. As the thermal wind is calculated in a vertical column and not along the tilted axis of the height minima (Fig. 3b, left panel), Eqs. (5) and (6) will be negative in tilted conventional extratropical cyclones (Fig. 3b, right panel). Finally, as shown in Fig. 3a, the radius of 500 km is more than sufficient to resolve the full magnitude of the warm-core height perturbation associated with the vertically stacked tropical cyclone. The thermal wind parameters of Eqs. (5) and (6) can successfully resolve the phase of both tilted and vertically stacked cyclones, although structural changes beyond a radius of 500 km will not necessarily be indicated by the phase diagnostics if those changes are not communicated to smaller radius.

Since all three diagnostics can be evaluated using solely the three-dimensional height field (and the MSLP field to track the cyclone), they have broad potential use in both the research and operational forecast communities (section 6). It is essential to point out here that the cyclone phase diagnostics just described will only be as accurate as the model analyses or forecasts from which they were derived. The cyclone that is represented within the model analysis or forecast cannot be a completely accurate representation of the cyclone's true three-dimensional geopotential field, although advances in data assimilation techniques over the past decade have improved analysis and forecast quality (Caplan et al. 1997; Velden et al. 1998a). Thus, while the phase diagnostics and the resulting diagrams provide critical in-

sight into the cyclone structure and intrinsic phase, they must be compared with direct observations, including satellite images, satellite-derived diagnostics (e.g., Dvorak 1984; Hebert and Poteat 1975; Velden et al. 1998b), surface and upper-air observations (when available), and Advanced Microwave Sounding Unit (AMSU) thermal profiles (Brueske and Velden 2000; Kidder et al. 2000). Only through a synthesis of all these observations and diagnostics can the most accurate insight into cyclone phase evolution be obtained. These diagnostics are intended to supplement existing methods. It is also important to note that tracking errors, while unusual given the tracking method complexity described in section 2, will lead to phase diagnostics (especially for parameter B) that may not be representative of the actual cyclone.

b. Cyclone phase diagram construction

The three diagnostics above [Eqns. (2), (5), and (6): parameters B , $-V_T^L$, and $-V_T^U$, respectively] define the three-dimensional cyclone phase space. Since a three-dimensional cube is cumbersome to visualize readily, the phase space is presented using two cross sections through the cube: B versus $-V_T^L$ and $-V_T^U$ versus $-V_T^L$, examples of which are shown in Figs. 4a and 4b, respectively. In Fig. 4a, leftward motion indicates an increased cold core (or weakening warm core). Upward motion in Fig. 4a indicates increasing thermal asymmetry. In Fig. 4b, motion toward the lower left indicates increasing cold-core strength and depth (or weakening warm-core strength and depth).

The full life cycle of a cyclone is defined through the trajectory through the phase diagram, with time moving forward as one moves along the trajectory, from the labeled A to Z [not labeled in Fig. 4 as those points coincide near coordinates (0,0), but they are labeled in successive phase diagrams, Figs. 5–8]. For each of the three phase parameters, a 24-h running mean smoother is applied to remove short-term noise in the evolution resulting from the coarse grid resolution of the gridded analyses and the inability to diagnose cyclone movement between grid points. The shading of the markers corresponds to the intensity of the cyclone (in hPa), with white as the weakest (>1010 hPa) and black as the most intense (<970 hPa). The size of the cyclone (mean radius of the 925-hPa gale force wind field area) is represented by the size of the solid circle marker along the phase trajectory (largest shown in Fig. 4 is approximately 600 km). The track of the cyclone is plotted in the inset, with the 0000 UTC positions marked. The start of the cyclone life cycle is given by the A, while the end of the cyclone life cycle is given by the Z. These points are not necessarily the formation and decay points of the cyclone, but represent the start and end of the cyclone life cycle resolvable within the available dataset and its geographic boundaries. If the phase diagram includes forecast data, the current (analyzed) location

within the phase space is given by the C (not shown). The resulting objective phase diagram is qualitatively similar to the subjective diagram proposed by Beven (1997, his Fig. 5), although the placement of cyclone types within that diagram differs from Fig. 4, based upon the parameters chosen here.

c. Datasets

1) CASE EXAMPLES OF PHASE EVOLUTION

Several dozen cyclones of highly varied phase and intensity since 1948 were examined using several datasets. From 1948 through 1999, global 2.5° reanalysis fields from the NCEP–NCAR reanalysis (Kalnay et al. 1996) were used for cyclone life cycle analysis. During the 1979–93 tropical cyclone seasons, global 1.125° reanalysis fields from the ECMWF reanalysis (Gibson et al. 1997) were used. Both the NCEP–NCAR and ECMWF reanalyses have the benefits of higher temporal resolution (6 h) and an analysis method that is consistent over the dataset period. Neither reanalysis uses a synthetic vortex (bogus) for tropical cyclones, but rather rely upon satellite-derived thermal and moisture profiles, in situ surface data, and model first guess to produce a reasonable estimate of the tropical cyclone structure at the coarse grid resolution.

From 1998 through 2001, higher-resolution (1°) operational analysis from the Navy Operational Global Atmospheric Prediction System (NOGAPS) model (Hogan and Rosmond 1991) were used for cyclone analysis. Equivalent cyclone analyses were performed using 1° NCEP Aviation Model (AVN; Kanamitsu 1989) and 1.25° U.K. Met Office (UKMET; Cullen 1993) model analyses to illustrate the robust nature of the diagnoses as resolution and model initialization varies (not shown but available online at <http://eyewall.met.psu.edu/cyclonephase>). For example applications of the phase diagram in a forecast setting (section 6), operational output from the NOGAPS, AVN, UKMET, and Canadian Meteorological Centre (CMC) Global Model (Côté et al. 1993, 1998a,b) were used. It is important to note that with the exception of the 2001 AVN analyses, all the operational forecast data used incorporated a synthetic vortex (bogus) for tropical cyclone initial conditions to produce a more accurate estimate of the tropical cyclone intensity. This bogus was typically the strongest in NOGAPS, and weakest in the CMC and UKMET models. The impact of the bogus on phase diagnosis has not yet been fully evaluated, but preliminary results indicate that a strong bogus leads to a more symmetric, stronger warm-core phase using the definitions just described (Evans and Hart 2003). These datasets are summarized in Table 2.

Sea surface temperature analyses were derived from the Reynolds weekly averaged 1.0° SST field for the period 1982–2000 (Reynolds and Smith 1995), when corresponding higher-resolution operational analyses

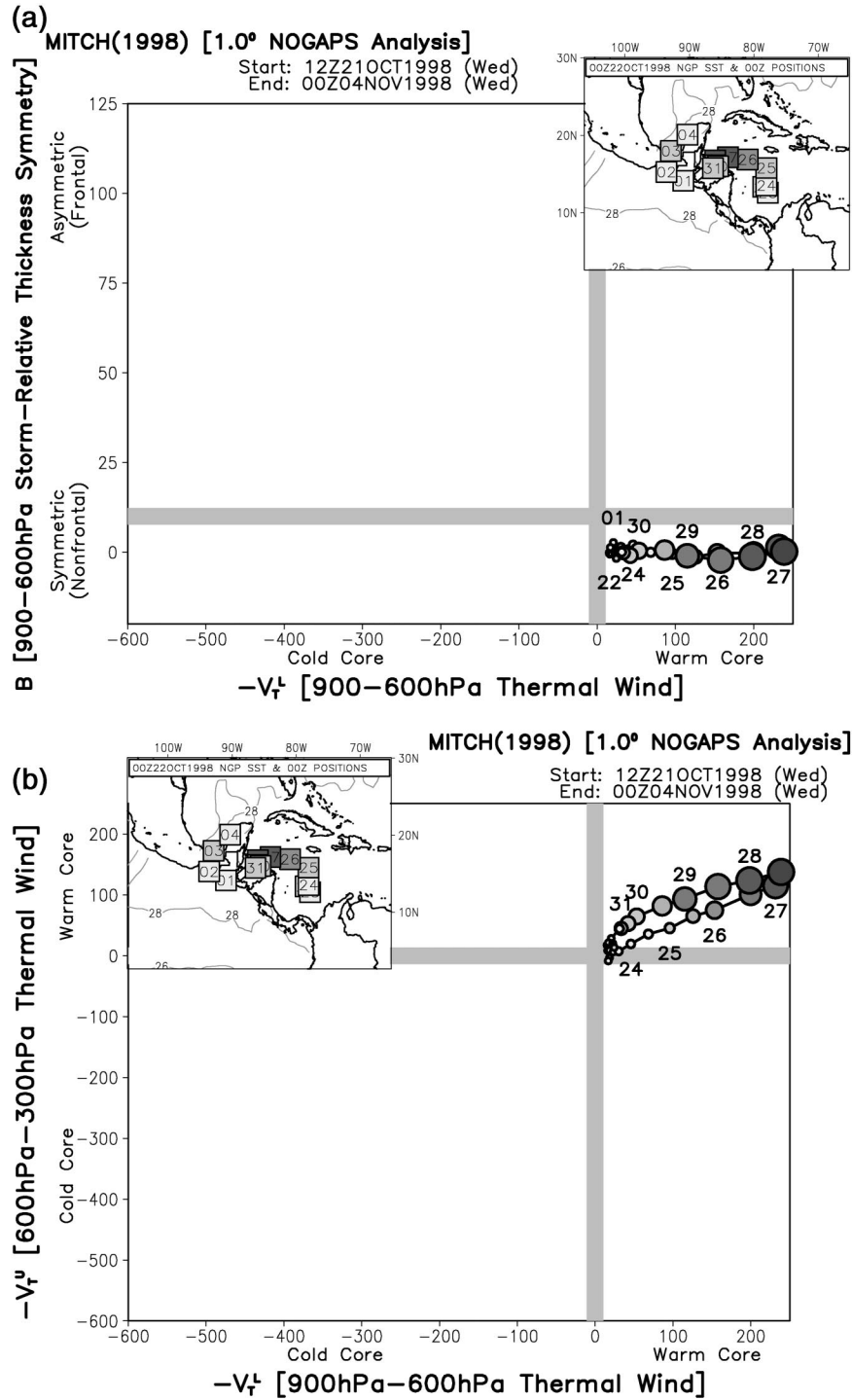


FIG. 4. Proposed cyclone phase diagram. Example here is for a symmetric warm-core cyclone (conventional tropical cyclone, Hurricane Mitch from 1998 using 1° NOGAPS analyses every 12 h). Phase evolution: (a) $-V_r^z$ vs B and (b) $-V_r^z$ vs $-V_r^u$. The inset gives the track of the cyclone and the model analysis SST field (°C). The A indicates the beginning of the plotted life cycle within the available analyses and the Z indicates the end [not shown here for clarity, as those two points coincide near (0, 0) in both figures; they are labeled in successive phase diagrams]. A marker is placed every 12 h. The shading of each marker indicates cyclone MSLP intensity (white, >1010 hPa; black, <970 hPa) and the size of the circular marker within the phase space indicates the relative size (mean radius) of the 925-hPa gale force (>17 m s⁻¹) wind field (largest here is 600 km). Positions at 0000 UTC are labeled with the day. The upward growth, then decay, of the thermally symmetric warm-core vortex is illustrated.

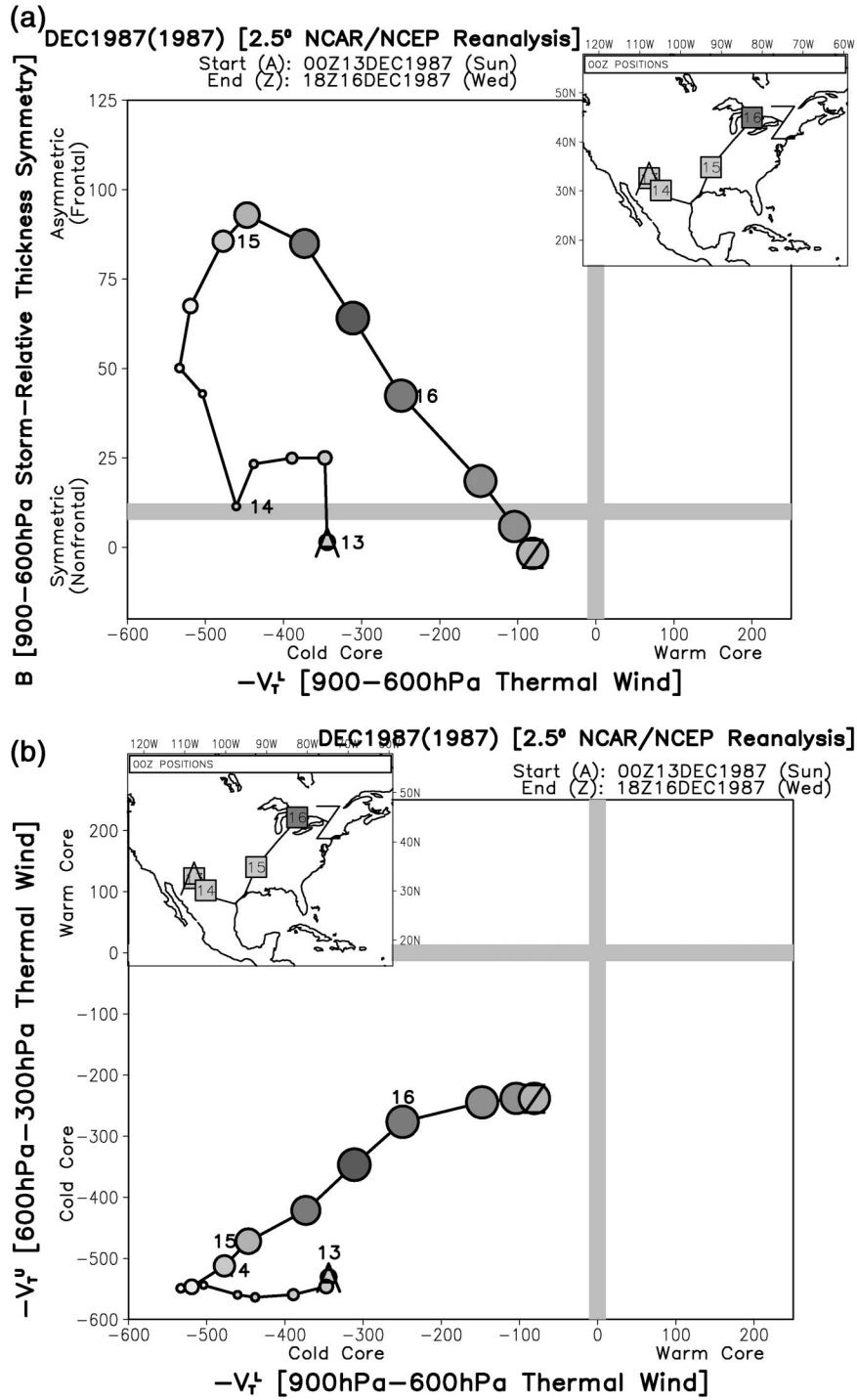


FIG. 5. As in Fig. 4 except for the life cycle evolution of a cold-core cyclone [conventional extratropical cyclone, 13–16 Dec 1987 case from Schultz and Mass (1993)] using 2.5° NCEP–NCAR reanalyses. The development of a highly frontal, cold-core cyclone that ultimately occludes is illustrated. Each marker represents a 6-h increment, the temporal resolution of the NCEP–NCAR reanalysis dataset. The cold-core structure of the cyclone weakens as intensification occurs since the cyclone is becoming almost vertically stacked.

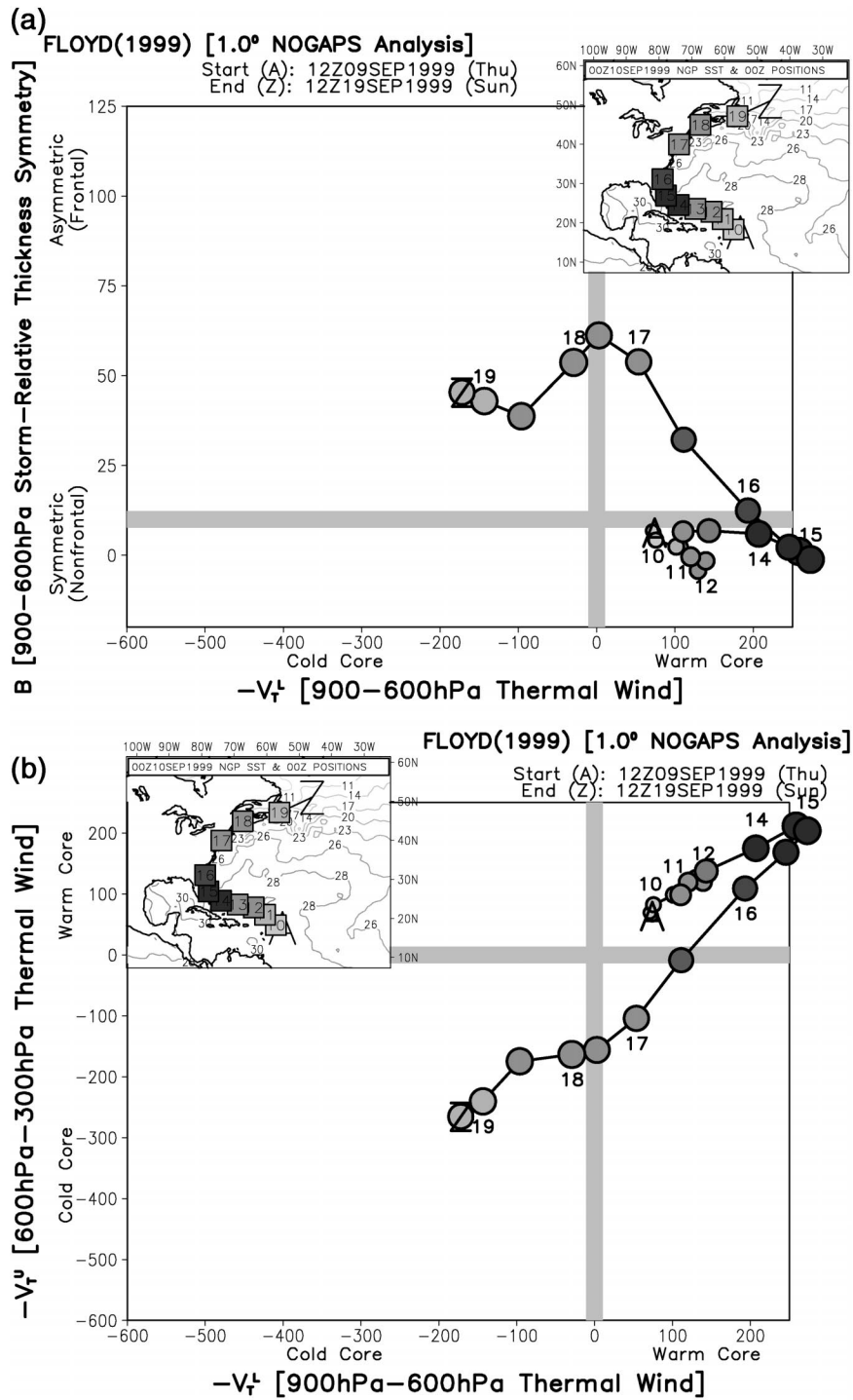


FIG. 6. As in Fig. 4 except for the life cycle evolution of an extratropically transitioning tropical cyclone (Hurricane Floyd from 1999) using 1° NOGAPS analyses every 12 h. The conversion of a thermally symmetric, deep strong warm-core cyclone into a frontal cold-core cyclone is illustrated. The cyclone exists as a hybrid cyclone (frontal warm core) for a substantial period of time during extratropical transition.

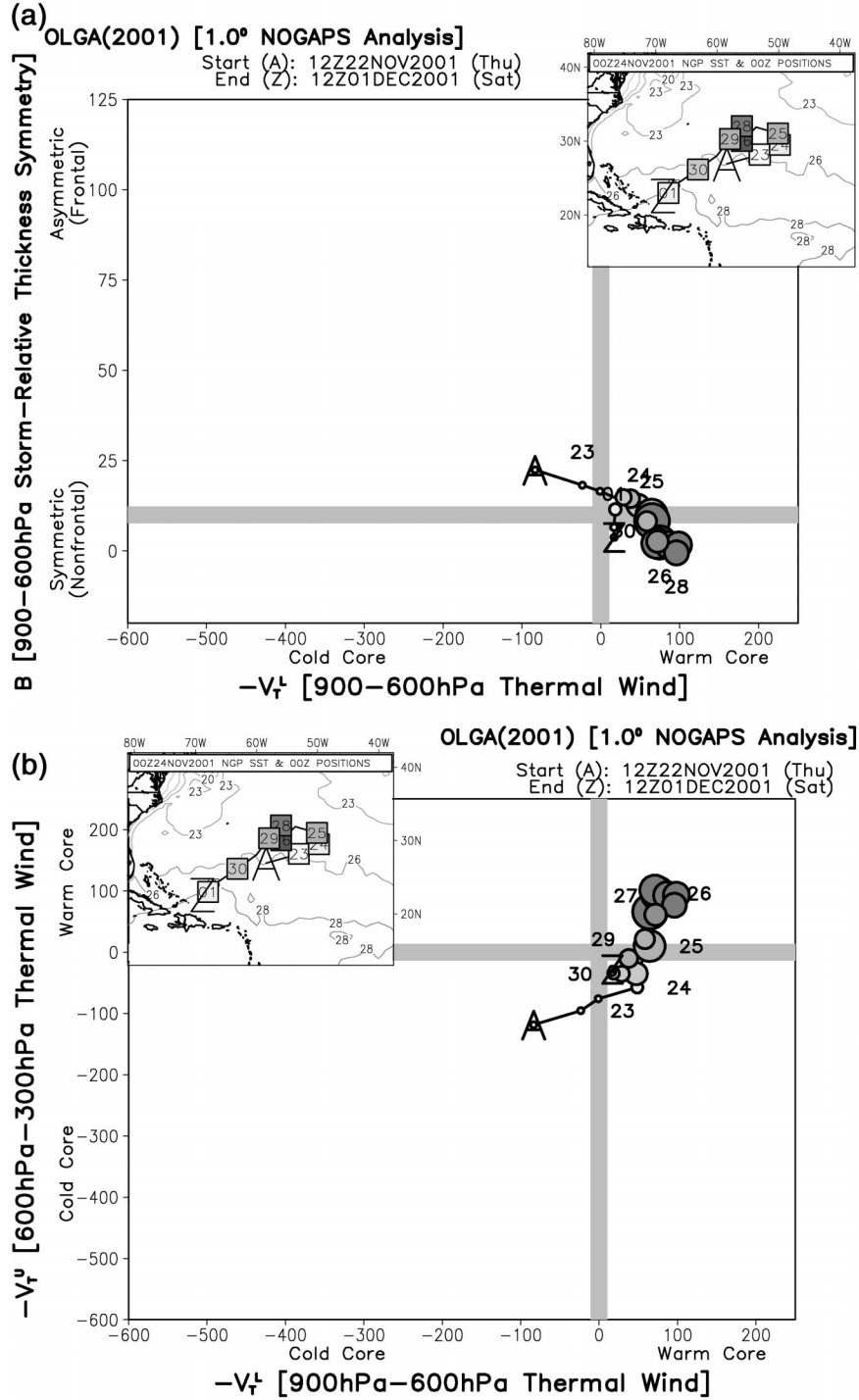


FIG. 7. As in Fig. 4 except for the life cycle evolution of the tropical transition of a nontropical cyclone (conversion of a weak extratropical cyclone into subtropical storm 2 and then finally Hurricane Olga from 2001) using 1° NOGAPS analyses every 12 h. The conversion of a lower-tropospheric cold-core cyclone into a warm-core cyclone is illustrated, followed by the upward growth of the shallow warm-core (subtropical) cyclone into a tropical cyclone. This was one of two cases in 2001 whose transition from subtropical to tropical cyclone was forecast using similar phase diagrams produced from model forecast output.

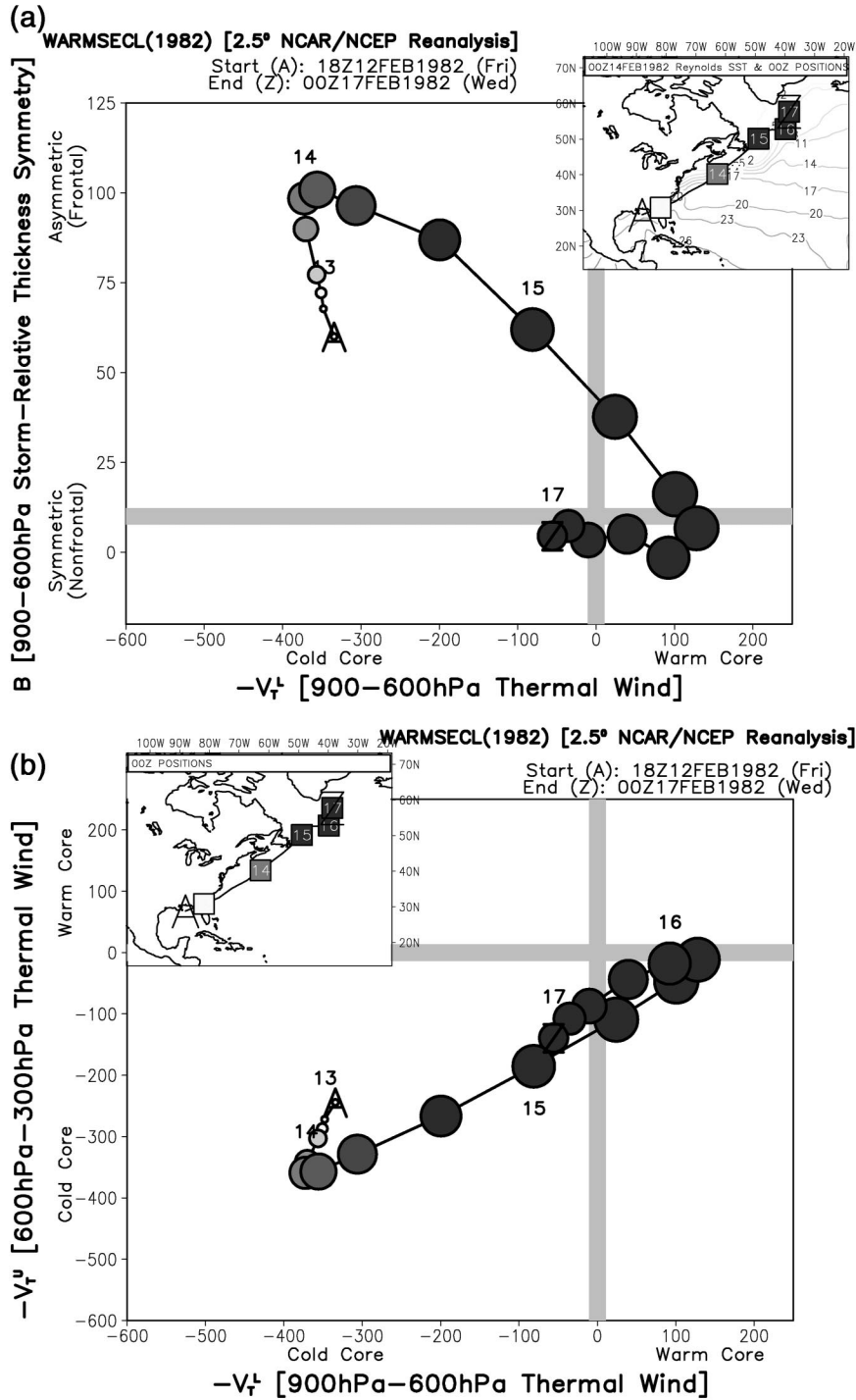


FIG. 8. As in Fig. 4 except for the life cycle evolution of an extratropical cyclone that undergoes a warm seclusion [the *Ocean Ranger* storm of 12–17 Feb 1982 examined in Kuo et al. (1992)] using 2.5° NCEP–NCAR reanalyses every 6 h. The development of a symmetric, warm-core structure between 900 and 600 hPa illustrates the warm-seclusion phase between 15 and 16 Feb 1982. A major phase distinction between the diagnosed warm-core structure here (warm seclusion) and that in a mature tropical cyclone (Fig. 4) is the lack of warm-core structure above 600 hPa.

were not available. Analyses and phase diagrams for cyclones shown here and others are available via the World Wide Web (<http://eyewall.met.psu.edu/cyclonephase>).

2) PHASE CLIMATOLOGY

In section 5, a climatology of cyclone phase is performed using over 17 000 cyclones over the period 1980–99. For this extended period of time, the 2.5° NCEP–NCAR reanalysis fields described above were used. Given the resolution of the all datasets used here, it follows that cyclones of smaller scale will be less accurately analyzed than cyclones of larger scale [in particular, the calculation of Eqs. (5) and (6) for the 2.5° NCEP–NCAR reanalyses]. As a result, there will be an inherent bias in the datasets toward underestimating the intensity and warm-core structure of tropical cyclones, with a reduced bias expected for extratropical cyclones.

The insight provided by phase evolution is now illustrated for several types of both conventional (single phase) and unconventional (multiple phase) cyclones.

3. Conventional (single phase) life cycles

Textbook examples of the conventional (single phase) life cycles of extratropical and tropical cyclone development are shown below. These cyclones are conventional (or stereotypical) in that the extratropical cyclone life cycle is completely cold core while the tropical cyclone life cycle is completely warm core; there is no overlap in phase. Both cyclones reach intensities within the available gridded analyses that are typically strong, but not excessive to invalidate their representativeness as case studies.

a. Symmetric warm-core development: Tropical cyclone life cycle—Hurricane Mitch, 1998

The conventional warm-core life cycle of a tropical cyclone within the phase space is illustrated by Hurricane Mitch from 1998 in Fig. 4, using 1° NOGAPS analyses every 6 h. A detailed analysis of Mitch's formation and evolution is given by Guiney and Lawrence (1999). Although Mitch in reality attained record low MSLPs (Guiney and Lawrence 1999), the coarse NOGAPS analysis resolved the cyclone's peak intensity only around 977 hPa, making it a warm-core cyclone of typical tropical cyclone intensity (category one hurricane) suitable for the conventional illustration here. Operational analyses of tropical cyclones today may be more successful at resolving the actual intensity of tropical cyclones through more sophisticated bogusing and data assimilation techniques.

This traditional warm-core life cycle begins with the formation of a tropical depression over water of temperature 26°C or greater on 22 October 1998. This depression has a cyclone phase that is thermally symmetric

(nonfrontal) ($B = 0$; Fig. 4a) and weakly warm core in the lower troposphere ($-V_T^L \approx +10$; Figs. 4a,b). The warm core has not yet built upward to 300 hPa, however ($-V_T^U \approx -10$; Fig. 4b), typical of most tropical depressions or weak tropical storms resolved at 1° resolution. As tropical cyclone intensification occurs, surface fluxes of moisture and heat, and the resulting latent heat release from convection, drive a vertical profile of negative height tendency whose magnitude is maximized just above the surface and decreases upward (Charney and Eliassen 1964; Ooyama 1969; Emanuel 1986; Rotunno and Emanuel 1987; see also Fig. 4). The strengthening vortex further allows the lower-tropospheric warming (resulting in the hydrostatic lowering of the height field) to be inertially restricted within the core [increasing ΔZ , Eq. (3)], rather than being radiated outward by gravity waves (Shapiro and Willoughby 1982). The increasing symmetry of the system is realized as a consistent near-zero value of B (Fig. 4a), with a well-defined maximum of thickness near the cyclone core that decreases outward in all directions (e.g., Fig. 2a). The warm core that was initially confined to the lower troposphere on 22 October has extended up to 300 hPa by 25 October ($-V_T^U$ now positive; Fig. 4b). This extension of the warm core upward results from sustained convection producing deep tropospheric warming within the core of the cyclone (in addition to subsidence within the eye that cannot be resolved within the gridded analyses used here), leading to a hydrostatic lowering of isobaric heights up to 300 hPa. The cyclone is now diagnosed as deep warm core, typical of strong tropical storms and hurricanes.

Further warm-core intensification during the last week in October is illustrated as a rightward movement to a stronger tropospheric warm-core structure ($-V_T^L \approx +250$ and $-V_T^U \approx +150$) with nearly perfect (within the resolution of the analyses) symmetric structure ($B = 0$). Consistent with a full-troposphere warm-core structure, $-V_T^L$ remains larger than $-V_T^U$ throughout the life cycle. The hydrostatic relationship dictates that the height perturbation on an isobaric surface is related to the net virtual temperature perturbation above that surface. As one moves downward in a tropical cyclone, the net temperature perturbation becomes increasingly positive, leading to an increasing height perturbation (ΔZ) and a value of $-V_T^L$ that is necessarily larger than $-V_T^U$. If the energy source remains sufficient and the warm-core cyclone is not impacted by shear, dry air, or land, it can continue to intensify its warm-core structure, bound theoretically only by frictional dissipation (Emanuel 1988; Bister and Emanuel 1998). One interesting area of future research is to determine the theoretical maximum magnitudes of $-V_T^L$ and $-V_T^U$ that are associated with a tropical cyclone that has approached the extreme maximum potential intensities (MPIs; Emanuel 1988) for tropical cyclones. The values of $-V_T^L$ and $-V_T^U$ over 200 at 1° grid resolution for a 980-hPa Mitch in Fig. 4a lead to speculation that at much

higher resolution a tropical cyclone of 900-hPa intensity or greater would produce values of $-V_7^L$ and $-V_7^U$ in excess of 500.

Mitch reached peak intensity (977 hPa on the 1° NO-GAPS analysis) on 27–28 October 1998, and then weakening of the tropical cyclone ensued as Mitch encountered land. In the absence of trough interaction, the decaying cyclone generally retraces its path backward within the phase diagram as the warm-core symmetric structure weakens. As land is the source of weakening in this case, $-V_7^L$ weakens more rapidly than $-V_7^U$ (Fig. 4b). When shear or trough interaction weakens the tropical cyclone, $-V_7^L$ usually weakens more slowly than $-V_7^U$ (see section 4a and Fig. 4b).

The vast majority of eastern Pacific tropical cyclones, and a smaller fraction of Atlantic tropical cyclones, have a phase diagram life cycle qualitatively similar to Mitch, although most are not as strong. This simple tropical cyclone life cycle occurs only in the absence of trough interaction and extratropical transition, which can produce a phase diagram life cycle that is considerably more complex, as is often the case in the Atlantic basin or western Pacific basin (section 4a).

b. Asymmetric cold-core development: Extratropical cyclone life cycle, 14–16 December 1987

A case of a conventional extratropical cyclone life cycle (single phase: cold core only) is shown using a previously well-studied case of cold-core development over land in December 1987. Mass and Schultz (1993) and Schultz and Mass (1993) found this event to be a classic case of occlusion, without the development of a warm seclusion that is more typical of intense maritime cyclones (section 4c). The surface cyclone forms in a weakly baroclinic environment in western Texas on 13 December ($B < 25$ in Fig. 5a). As an upper-level shortwave advances on the weak surface cyclone (not shown), the middle- and upper-tropospheric height gradient above the surface cyclone intensifies (isobaric heights decrease) more rapidly than near the surface, leading to an increasing cold-core cyclone signature ($-V_7^L$ becomes more strongly negative on 13 and 14 December). This impact of the shortwave on the lower-middle troposphere is shown as leftward movement in the phase diagram on 13–14 December. Concurrent with the increasing cold-core signature is the increasing thermal asymmetry of the cyclone [B ; Eq. (2)], as evidenced by the upward component to the cyclone phase trajectory in Fig. 5a. As B increases, cold air advects into the rear of the cyclone while warm air advects poleward to the right of the cyclone motion, consistent with a thermally direct circulation in the Northern Hemisphere.

On 15 December the surface cyclone intensifies rapidly, and the cold-core structure weakens. The amplification of the surface wave by the upper-level trough weakens the cold-core structure since the surface height field amplifies more rapidly than the middle- or upper-

troposphere height field. This is presumably a consequence of the baroclinic wave reaching a horizontal tilt that maximizes the growth rate as described by instability theory (Charney 1947; Eady 1949). As the lower-tropospheric cyclone intensifies, rapid movement to the right and downward within Fig. 5a and to the right and upward within Fig. 5b is observed. The cyclone becomes less thermally asymmetric as the instability is removed (B decreasing in Fig. 5a). Through ageostrophic ascent-induced cooling, the tilted cold-core structure of the cyclone continues to weaken as the lower-tropospheric height gradient reaches a magnitude consistent with the middle- and upper-tropospheric height gradient, which is also consistent with a near vertical stacking of the cyclone.

Maximum intensity of the surface cyclone (approximately 982 hPa on the 2.5° NCEP–NCAR reanalysis) occurs at 1800 UTC 15 December. Late on 16 December, the cyclone has occluded ($B \approx 0$) with a greatly weakened cold-core structure ($-V_7^L \approx -75$). Now vertically stacked, the height gradient in the lower troposphere is nearly the same as the magnitude in the middle troposphere. In the absence of further forcing (through either increased surface fluxes or another trough interaction), the cyclone has lost its ability for further intensification. Following occlusion, cold air has wrapped partially around the east side of the cyclone while warm air has wrapped to the north of the cyclone (Mass and Schultz 1993; Schultz and Mass 1993). As a result, the cyclone has a weak negative value of B at 1800 UTC 16 December and is typical of the thermally indirect occlusion phase of extratropical cyclones. In the conventional extratropical life cycle, the cyclone will ultimately weaken to an open wave, be absorbed by another upstream extratropical cyclone, or provide the forcing for additional cyclogenesis. This latter point also illustrates the difficulties in cyclone tracking discussed in section 2a.

4. Unconventional (multiple phase) life cycles

The cases of cyclone life cycle described in section 3 conform to textbook examples of extratropical and tropical cyclone development, maturity, and decay. They represent cyclones where the distinction between extratropical and tropical phases are clearly discernible. However, many cyclones in the atmosphere do not have such clearly defined boundaries. Over the past several decades it has become increasingly apparent that cyclone life cycles can involve many phases and can readily cross the artificial boundary between cold core and warm core ($-V_7 = 0$). Examples of such unconventional life cycles—where multiple phases are observed for one cyclone—are given below.

a. Warm- to cold-core transition: Extratropical transition of Hurricane Floyd, 1999

The evolution of Hurricane Floyd in 1999 from intense tropical cyclone into an extratropical cyclone

(Lawrence et al. 2001) is shown here through phase analysis (Fig. 6) as a typical example of extratropical transition. Although Floyd represents a classic case of transition, it cannot represent the full range of observed extratropical transition cases. The life cycle of Floyd in Fig. 6 begins on 9 September, 1 day after tropical cyclogenesis (Lawrence et al. 2001). Through 15 September, Floyd undergoes classic symmetric warm-core development as discussed in section 3a, and at peak tropical intensity on 15 September 1999, Floyd is resolved using 1° NOGAPS analyses with $-V_T^L \approx +250$, resembling Hurricane Mitch from Fig. 4.

A strong trough approaches the landfalling cyclone over North Carolina on 16 September (not shown; see Lawrence et al. 2001) and the cyclone begins conversion to an extratropical cyclone. This initiation is marked as B first exceeds 10 m (section 2a; see also Hart 2001; Evans and Hart 2003), early on 16 September. During 16 September the cyclone has become a frontal warm-core cyclone (hybrid), having characteristics of both tropical and extratropical cyclones that were apparent in satellite imagery animations (Evans and Hart 2003). At 1200 UTC 17 September, Floyd's warm core has reversed to cold-core structure ($-V_T^L$ first becomes negative; Figs. 6a,b), indicating transition completion (Hart 2001; Evans and Hart 2003), identical to the official declaration of extratropical transition as given in the tropical cyclone best-track dataset (online at <http://www.nhc.noaa.gov/1999floyd.html>). Thereafter, the cyclone intensifies its thermally asymmetric, cold-core structure through 20 September (Fig. 6). Although not shown, Floyd ultimately merged with another preexisting extratropical cyclone after 20 September. Figure 6b clearly shows that the transition to cold core as defined here occurred first in the upper troposphere and then worked downward later. This top-down transition of the cyclone is typical of trough interaction. It is unclear how a trough interaction that results in tropical cyclone intensification is represented within the phase analyses.

Floyd represents a case where extratropical transition occurs quickly enough that existence as a hybrid cyclone (frontal warm core; upper-right quadrant in Fig. 6a) was relatively short lived (approximately 24 h). In the absence of a strong trough, extratropical transition can take several days leading to a hybrid classification for an unusually long period of time (e.g., Hurricane Charley from 1986; see URL from section 2b). Further discussion of the range of synoptic evolution and diagnosis of extratropical transition can be found in Harr et al. (2000), Klein et al. (2000), Hart (2001), and Evans and Hart (2003).

b. Cold- to deep warm-core transition: Extratropical and subtropical to tropical transition of Olga, 2001

In the Atlantic basin slightly more than half of tropical cyclones form from tropical easterly waves moving off

the African coast [Elsberry (1995); e.g., Floyd from 1999 in section 4a]. Occasionally, tropical cyclones can form from a frontal wave or the conversion of an occluded cold-core cyclone or subtropical cyclone into a tropical cyclone. Atlantic Hurricanes Karen (not shown; see URL from section 2b) and Olga (Fig. 7), both from 2001, are examples of the latter. The case of Olga is shown here as a stereotypical example of the conversion of a nontropical cyclone into a tropical cyclone, and this transition was also well forecast by the operational models as viewed through the phase space derived from them, although it is beyond the scope of this paper to examine the forecast skill here.

A cyclone south of Bermuda on 22 November was diagnosed with a weak frontal cold-core structure (Fig. 7). Over a period of approximately 48 h, the low drifted northeastward and shear decreased (operational discussions from NHC, not shown). Surface fluxes of heat and moisture would lead to increased surface-based deep convection in this low-shear environment. This allowed the weak lower-tropospheric height perturbation to intensify and the initially cold-core structure was converted to neutral and then warm-core structure on 24 November ($-V_T^L > 0$ in Figs. 7a,b), although the 600–300-hPa layer remained cold core for another 24 h ($-V_T^L < 0$; Fig. 7b). Operationally, NHC diagnosed that a subtropical storm had formed at 2100 UTC 24 November (Hebert and Poteat 1975), consistent with the phase diagram lower-troposphere warm core, yet weakly frontal, diagnosis (Fig. 7).

On 24 and 25 November, the warm core continues to build upward and at 1200 UTC 25 November, a full-troposphere warm-core cyclone is diagnosed for the first time ($-V_T^L > 0$ in Fig. 7b). It would take another 24 h before NHC would operationally declare the cyclone to be tropical, although the best-track postanalysis is not yet available from NHC. The evolution on 24 and 25 November in Fig. 7b is typical of the conversion of a weak extratropical cyclone into a subtropical cyclone, and then finally into a tropical cyclone. This phase trajectory can be used as one method of guidance for anticipating such subtle subtropical to tropical development within model forecasts.

Tropical intensification accelerates and a relatively strong warm-core structure ($-V_T \approx +100$) was diagnosed on 26 and 27 November. Olga then began experiencing significant shear from the north (not shown), drifted southward, and decayed as a shallow, weak warm-core remnant low in early December.

c. Cold- to shallow warm-core transition: Warm seclusion within an extratropical cyclone—February 1982

Recently, an extension to the Bjerknes and Solberg (1922) extratropical cyclone life cycle was proposed that illustrates the development of a secluded region of warm air near the center of an intense extratropical cyclone

(Shapiro and Keyser 1990). Such warm seclusions have been found in midlatitude intense oceanic cyclones, in particular (e.g., Gyakum 1983a,b; Kuo et al. 1992). The warm seclusion develops as a result of rapid intensification, with cold air encircling the cyclone core so quickly that warm air ahead of the cold front is trapped near the cyclone core. This leads to a lower-tropospheric column of warm air over the surface cyclone center and further hydrostatic lowering of the height field and MSLP. The warm-seclusion process has been observed in adiabatic models of cyclone development (Reed et al. 1994) and, therefore, can occur in the absence of convection or surface fluxes; however, both of these diabatic processes can enhance the warm-seclusion process (Gyakum 1983a,b; Kuo et al. 1992).

The case of a warm-core extratropical cyclone shown in Fig. 8 is that examined in Kuo et al. (1992), the *Ocean Ranger* storm of February 1982 using 2.5° NCEP–NCAR reanalysis. On 12 February, the cyclone forms in a moderately cold core environment over the northern Gulf of Mexico (Fig. 8). On 13 February, an upper-level short wave moved into the base of a long-wave trough across the eastern United States (not shown; see Kuo et al. 1992), and $-V_7^L$ becomes increasingly negative, consistent thus far with the conventional extratropical cyclone evolution described in section 3b. On 14 February, explosive development occurs. This case departs from conventional extratropical development (section 3b) since the cyclone lower-tropospheric structure becomes warm core on 15 February, which then intensifies dramatically ($-V_7^L > +150$). While an impressive lower-tropospheric warm-core structure develops, the troposphere above 600 hPa (Fig. 8b) remains neutral phase at best through early on 16 February. The vast majority of warm seclusions examined have a warm core that is confined to below 600 hPa. Only in the most intense of warm seclusions (intensity below 940 hPa at 2.5° resolution) does $-V_7^L$ become slightly positive, possibly as a result of a lowering of the tropopause well below 300 hPa in association with such an intense high-latitude cyclone. This is one major phase distinction between tropical cyclones and warm-secluded extratropical cyclones, in that by definition a well-resolved tropical cyclone has a full-troposphere warm-core phase.

Once the warm seclusion is achieved, it can remain so for a substantial period of time (e.g., 60 h in Fig. 8). However, the vertical stacking that results from the warm seclusion means that baroclinic development generally ceases and a slow weakening begins. As the cyclone begins to weaken, cold advection of air eventually reaches the warm seclusion of the cyclone and the warm-core structure is converted back to a cold-core structure (1200 UTC 16 February). There are exceptions to the postseclusion weakening, including 1) if the warm seclusion is over sufficiently warm water that the warm core deepens to the tropopause from deep convective development, leading to potential tropical cyclone development, or 2) another short- or long-wave trough

interacting with the secluded cyclone, leading to further baroclinic or hybrid development from the newly regained tilt.

5. Phase climatology

a. Phase space inhabitance and intensity distribution

Although the examples shown in section 3 and 4 represent the dominant synoptic-scale cyclone types on Earth, five cases clearly cannot illuminate the relative frequency of cyclones observed. To provide insight into the visitation to each quadrant of the cyclone phase space, over 17 000 cyclones within the 2.5° NCEP–NCAR reanalyses having a life span of at least 24 h between 1980 and 1999 were classified within the phase space. This analysis was limited to the region between 120°W–0° and 10°–70°N. The resulting binned frequency distribution (Fig. 9) shows that developing and occluded cold-core cyclones are the most frequently occurring. Strongly frontal, warm-core cyclones ($-V_7^L > 0$ and $B > 0$) are rare (e.g., 1200 UTC 15 February within Fig. 8a); however, when they do occur they are most often intense (Fig. 10; mean intensity distribution). It is immediately apparent when examining 2.5° resolution data that it is exceptionally rare for a cyclone to achieve a value of B greater than 100 or a value of $-V_7^L$ or $-V_7^U$ less than -600 or greater than 200. As shown in sections 3a and 4a, it is possible using higher-resolution (1°) analyses to obtain higher values of $-V_7^L$ associated with strong tropical cyclones. Given the resolution of the analyses used here (2.5° NCEP–NCAR reanalyses), the occurrence of tropical cyclones within the phase space is greatly underestimated. This is particularly evident by noticing the near-complete absence of full-troposphere warm-core cyclones in the upper-right quadrant of Fig. 9b. However, the tropical cyclone examples shown in sections 3 and 4, combined with additional examples found at <http://eyewall.met.psu.edu/cyclonephase>, indicate that the deep warm-core tropical cyclone structure can be resolved by gridded data of 1°–1.25° resolution or finer. This result may have significant bearing on the ability to reliably determine the climatology of tropical-cyclone-like vortices and their full-troposphere warm-core structure in climate models that have resolution coarser than 2°.

Within the cold-core half of Fig. 9a ($-V_7^L < 0$) the axis of maximum frequency lies diagonally to the upper left. In contrast, the axis in the warm-core half of the phase diagram ($-V_7^L > 0$) lies horizontally near $B = 0$ in Fig. 9a. The latter argues that the development of a warm-core structure is most often associated with non-frontal (symmetric) structure. Another interpretation would be that a consequence of warm-core development is the eventual loss of thermal asymmetry (fronts). Given the necessary lack of tropical cyclones in Fig. 9, this would presumably be the climatology of warm-seclusion extratropical cyclones (e.g., Fig. 8).

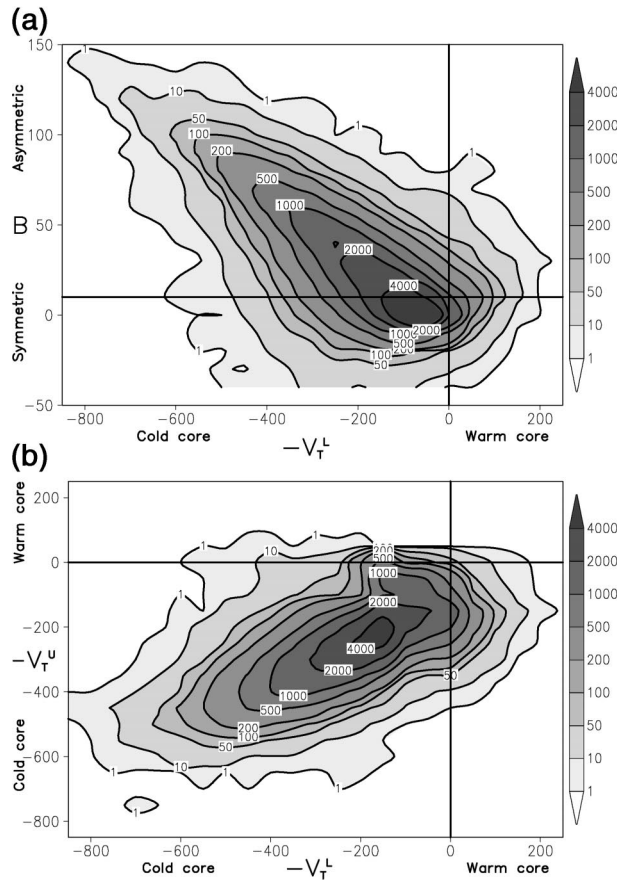


FIG. 9. Binned frequency distribution of phase space occurrence for (a) $-V_T^L$ vs B and (b) $-V_T^L$ vs $-V_T^U$. Note that the phase space domain shown here has been expanded over the domain shown in Figs. 4–8. Approximately 17 000 cyclones between 1980 and 1999 were examined using 6-hourly NCEP–NCAR reanalyses over the region from 10° – 70° N to 120° W– 0° to arrive at the unsmoothed distribution shown. Given the 2.5° grid resolution, the frequency and strength of deep warm-core cyclones [upper-right quadrant in (b)] is greatly underestimated. The true tropical cyclone structure shown in Fig. 4 (using higher-resolution analyses) cannot be represented by the 2.5° analyses used here. Thus, the distribution shown here represents the phase occurrence of cyclones in the northern Western Hemisphere, excluding tropical cyclones.

As discussed in section 2, there are five small regions of the domain where falsely detected cyclones are contributing to the frequency distribution in Fig. 9. These falsely detected cyclones are simply seasonal or climatological regions of lower MSLP, resulting from either a maximum of surface heating (e.g., Mojave Desert) or a terrain-induced elevated heat source that produces lower MSLP values from extrapolation below ground. While not shown here, examination of dozens of these cases in the phase space reveals they have structure that is near neutral (zero) for all three phase parameters or, at the most extreme, weakly shallow, symmetric warm core ($B \approx 0$; $-V_T^L \approx 25$; $-V_T^U \approx 0$). Thus, the frequency around the point (0, 0, 0) in Fig. 9 is likely slightly greater than should be expected for an analysis of true

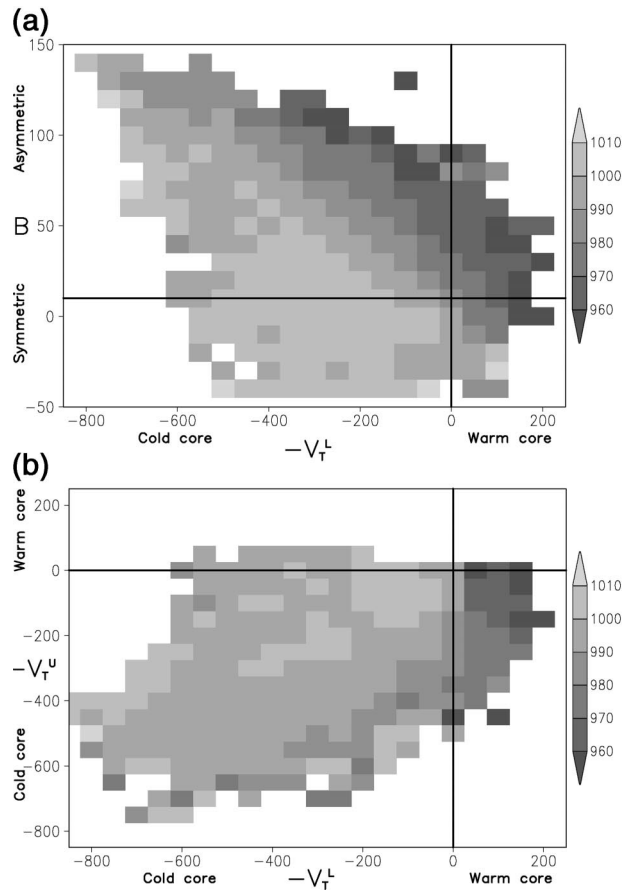


FIG. 10. As in Fig. 9 except for the mean cyclone intensity (minimum MSLP) as a function of phase space.

cyclones. However, since the frequency and areal coverage of these false cyclones is relatively small compared to the total domain frequency, the impact on the distribution in Fig. 9 is small. The region of the phase diagram distant from the origin is not influenced by these five regions of bogus cyclones given the typical phase structure of those bogus cyclones.

The examples and discussion in sections 3 and 4 implied a complex relationship between position within phase space and cyclone intensity. This relationship is most direct for warm-core cyclones and more complex for cold-core cyclones (Fig. 10). In section 3a it was shown that the cyclone intensity for a tropical cyclone is related to the magnitude of $-V_T^L$ and $-V_T^U$. As the warm-core cyclone intensifies, the distance from the origin (0, 0) in the figure increases (Figs. 4a,b). This is true since conventional tropical cyclone intensification enhances rather than removes the instability that is intensifying the storm in the first place (Charney and Eliassen 1964; Ooyama 1969; Emanuel 1986; Rotunno and Emanuel 1987). Therefore, as shown in Fig. 4, the cyclone intensity generally increases as the warm-core strength increases. This warm-core-intensity relation-

ship would be shown in Fig. 10 if tropical cyclones could be adequately resolved.

As discussed in section 3b, a less direct relationship exists between phase space location and intensity for cold-core cyclones (Fig. 10). As an extratropical cyclone intensifies, it necessarily removes through ageostrophic motions the internal instability that generated it. In the process of this stabilization, the cyclone tilt decreases, leading to a decrease in the cold-core strength. Thus, the location within the phase space for cold-core cyclones is more closely related to the point along the cyclone life cycle: formation, developing, maturity, or decay. A 995-hPa cyclone that has reached peak intensity may reside in the same location on the phase space as a 970-hPa cyclone that has reached peaked intensity since their cold-core structures (as defined here) may be the same. Since there are other factors dictating extratropical cyclone intensity (section 5b), there cannot be a one-to-one relationship between cyclone phase space location and cold-core cyclone intensity.

It follows that for cold-core cyclones, the distribution of mean intensity change (which is related to the stage of cold-core cyclone evolution) is much more insightful (Fig. 11). Consistent with our understanding of baroclinic cyclone development on fronts, the larger the thermal gradient across the cold-core cyclone (approximately B in Fig. 11a), the greater the intensification to be expected in the mean. Figure 11b argues strongly that the phase of the 600–300-hPa atmosphere more greatly determines the intensification rate than the 900–600-hPa phase. As $-V_T^u$ becomes increasingly negative, the expected intensification increases. After peak intensity, the cold-core structure weakens and this stage is represented by the large area of near-zero mean intensity change in the center of the distribution of Fig. 11b.

The distribution of intensity change for warm-core cyclones in Fig. 11 supports the earlier argument that those warm-core cyclones resolved by 2.5° data are warm-seclusion extratropical cyclones that have peaked in intensity. The mean intensity change for warm-core cyclones in Fig. 11 is significantly positive (weakening), and weakening increases as the warm-core structure increases, consistent with the discussion in section 4c. The inclusion of tropical cyclone data would show a substantially different signal within the warm-core half of Fig. 11. If higher-resolution data were used (1.25° or finer), the warm-core distributions shown in Figs. 9–11 would likely be significantly different.

As described above, the strong physical consistency of the intensity change distribution shown in Fig. 11 further argues that the chosen set of parameters successfully describes the life cycles of both cold-core and warm-core cyclones.

b. Phase space occurrence of rapid intensifiers

While the mean distributions shown in Figs. 9–11 are insightful, the nature of overlapping trajectories through

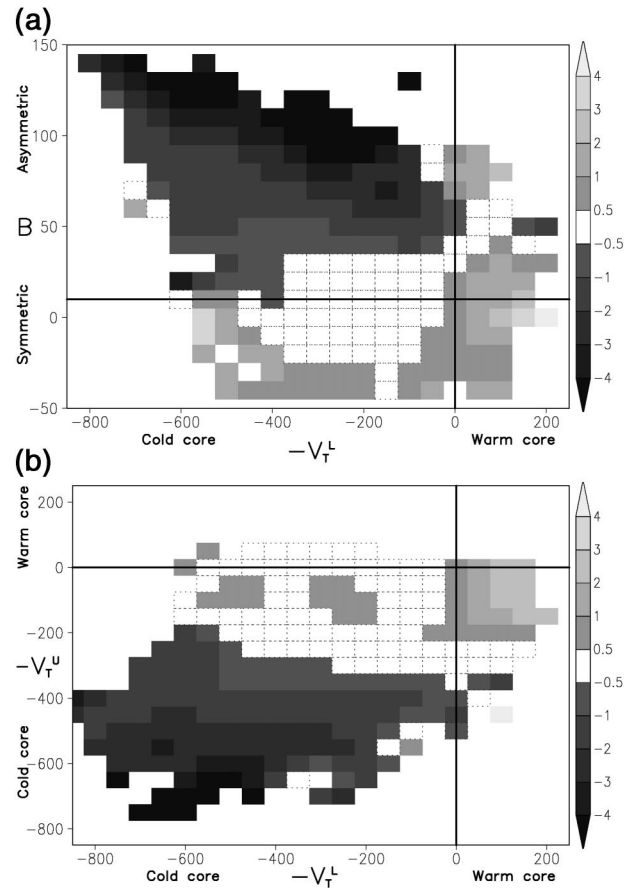


FIG. 11. As in Fig. 9 except for the mean 6-h pressure change (hPa) in cyclone intensity (minimum MSLP) as a function of phase space. The dotted boxes indicate the $(-0.5, 0.5)$ shading range in the legend.

the phase space (e.g., Fig. 8b) masks certain aspects of intensity change within the phase space. Of particular interest is the phase space occurrence of rapid intensifiers, defined as those that intensify by at least 24 hPa in a 24-h period (Sanders and Gyakum 1980). Those cyclones that meet this criteria in the 1980–99 2.5° NCEP–NCAR reanalysis dataset are shown in Fig. 12. The start of the 24-h period of rapid intensification is marked by an X, and the end of the period is marked by a filled circle. The majority of cyclones undergoing rapid intensification begin this process with moderate to high thermal asymmetry and a strong cold-core structure (Fig. 12a). Most revealing is that the majority of these events begin with the cold-core structure at lower levels being of similar magnitude to that at upper levels ($-V_T^L \approx -V_T^U$, Fig. 12b). Cyclones that have a cold-core structure that is not vertically uniform ($-V_T^L \ll -V_T^U$ or $-V_T^L \gg -V_T^U$) do not lead to rapid intensification. Thus, $-V_T^L \approx -V_T^U \ll 0$ is a necessary but, as will be shown below, not sufficient condition in phase space for rapid intensification. During the rapid intensification process, the cold-core structure weakens uniformly at both layers (Fig. 11b). This result is consistent

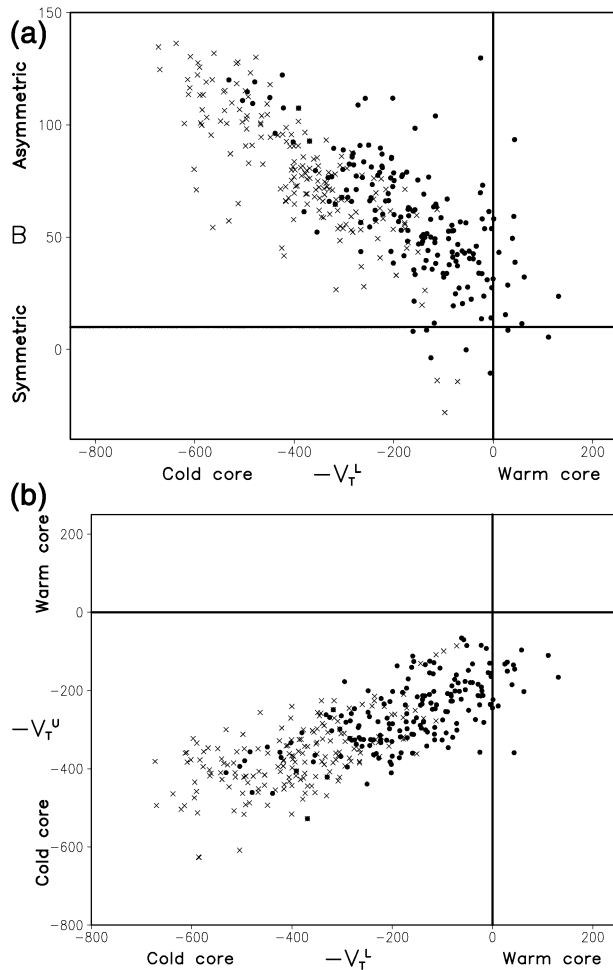


FIG. 12. Location of rapidly intensifying cyclones (at least 24 hPa day^{-1}) within the phase space for (a) $-V_T^L$ vs B and (b) $-V_T^L$ vs $-V_T^u$. The X marks the beginning and the filled circle (\bullet) marks the end of the 24-h period of rapid intensification.

with the ideal constructive interaction between forcing at the upper levels with forcing near the surface in baroclinic cyclogenesis. The distribution shown also indicates that the warm-seclusion phase sometimes occurs during the 24-h period of rapid intensification, but that it most often occurs after that 24-h period has ended, consistent with Fig. 11b.

Comparison of Figs. 9 and 12 indicates that the phase occurrence of rapidly intensifying storms falls closely to the maximum axis of phase occurrence for all cold-core cyclones. This result strongly argues that there are other factors in cold-core cyclone development that determine rapid intensity change than the three chosen here. These factors may include tropospheric static stability, boundary layer surface fluxes resulting from temperature and type of underlying surface, relative position of a lower-level cyclone with respect to an upper-level cyclone, and jet streak configuration, to name a few. Therefore, while the three chosen parameters are suc-

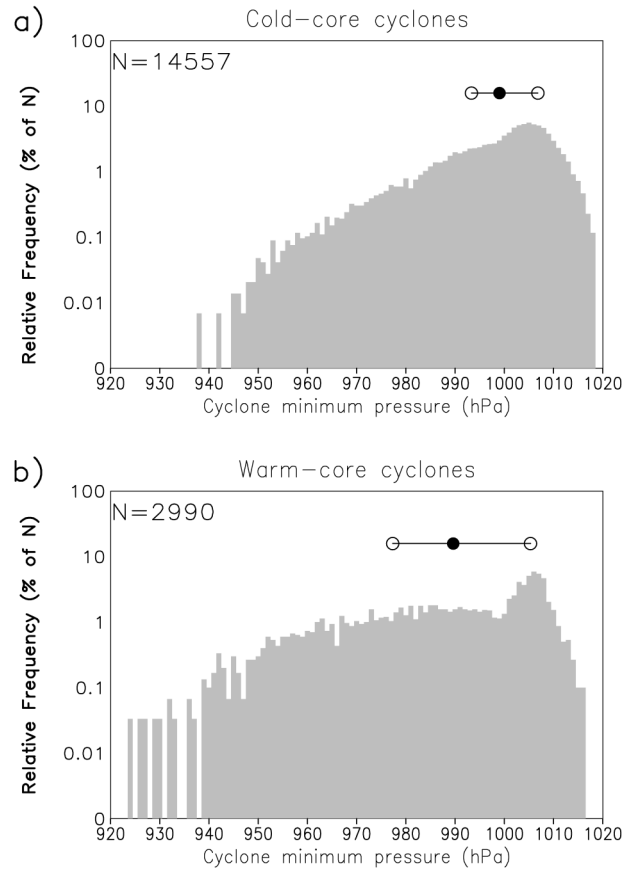


FIG. 13. Frequency distribution of cyclone peak intensity for (a) a cyclone never reaching warm-core structure and (b) cyclones reaching warm-core structure for at least 12 h. Note the scale shown is logarithmic. The number of cyclones in each group is labeled. The solid circle indicates the mean intensity, with the open circles indicating the first and third quartiles of the distributions. The lower end of the frequency distribution of (b) is greatly underestimated, since the 2.5° NCEP-NCAR reanalyses cannot adequately resolve tropical cyclones.

cessful at diagnosing the cold versus warm core and frontal phase of cyclones, as well as the stage of life cycle evolution for the majority of cold-core and warm-core cyclones, they are insufficient to diagnose the crucial characteristics unique to rapidly intensifying cyclones. The phase space as defined here cannot isolate the full necessary and sufficient conditions for rapid cold-core development. This result illustrates again that the full atmospheric cyclone phase space has many more dimensions than the three described here.

c. Comparison of intensity distributions between cold-core and warm-core cyclones

Figure 13 illustrates the intensity distribution disparity between cold- and warm-core cyclones for the domain described earlier. The mean peak intensity for cyclones that remain cold core is 10 hPa higher than that for cyclones that become warm core (solid circle su-

perimposed). This implies that, even though tropical cyclones are inadequately resolved at 2.5° resolution, the warm-core phase of cyclones is, on average, associated with a significantly stronger cyclone. Given the number and distribution of cyclones involved in Fig. 13, this mean peak intensity difference is statistically significant to the 99.9% confidence level.

As shown in Fig. 13, the maximum peak intensity observed at 2.5° resolution for purely cold-core cyclones is 938 hPa. The corresponding maximum observed intensity for cyclones that reach warm-core structure for at least 12 h is 924 hPa. Again, this result is without the inclusion of intense tropical cyclones, which may further increase the disparity of minimum intensity between the two phases given that the mean (and peak) tropical cyclone intensity is significantly more intense than that of extratropical cyclones. The large number of cyclones over the 20-yr period argues that an intensity below 940 hPa at 2.5° resolution over the North Atlantic and surrounding landmasses will be associated with the development of a warm-core structure within the cyclone for at least a 12-h period. Further, at 2.5° resolution, an intensity below 940 hPa will not occur without the presence of a warm seclusion. This result is further strengthened since the occurrence of warm-core cyclones is about one-fifth as common as that of cold-core cyclones. The range of intensity distribution (as given by the first and third quartiles in Fig. 13) is significantly larger for warm-core cyclones than purely cold-core cyclones, suggesting that the warm-seclusion phase of the extratropical cyclone may delay the normal occlusion process that rapidly weakens cold-core extratropical cyclones, although a detailed energetic analysis of many cases would be required to confirm this result.

While the intensity extrema statistics shown in Fig. 13 are significant and physically consistent, the specific thresholds discussed above are heavily resolution dependent. The comparison of maximum observed intensity for cold-versus warm-core cyclones is valid only for the 2.5° gridded data used. Higher-resolution data including manual analyses, allowing for the more accurate representation of tropical cyclones and warm seclusions, would lead to a warm-core distribution that has an even longer tail to higher intensity in Fig. 13. While higher-resolution data would alter the distribution of cold-core cyclones as well, it is reasonable to conclude that the change would be less dramatic. Cold-core cyclones, given their larger average size, are more accurately represented by 2.5° gridded data than warm-core cyclones. Thus, it is possible that higher-resolution gridded data would further strengthen the results shown in Fig. 13, illuminating an even larger intensity distribution and extrema difference between the two cyclone phases.

When long-duration higher-resolution global analyses (either manual or objective) become available, the diagnostics developed here could be used to estimate the actual observed lower bound of cyclone intensity for

purely cold-core cyclones. Such an empirical lower bound for cold-core cyclone intensity (based upon long-term sufficiently accurate and high-resolution analyses) would complement the well-established lower bound for warm-core tropical cyclone intensity determined both observationally (e.g., 870 hPa from Typhoon Tip in 1979) and theoretically (Emanuel 1988).

6. Operational guidance for forecasting phase evolution

To improve the real-time analysis and forecasting of cyclone phase, phase diagrams for current and forecast cyclones over the northeastern Pacific, North America, and the North Atlantic are provided through the World Wide Web (<http://eyewall.met.psu.edu/cyclonephase>). Cyclone phase diagrams are produced for all models for which sufficient gridded data are available: AVN, Canadian Meteorological Center Global Model (CMCGLB) and regional model (CMC's Global Environmental Multiscale Model, GEM), NCEP's Eta Model and Nested-Grid Model (NGM), U.S. Air Force Fine-scale fifth-generation Pennsylvania State University-NCAR Mesoscale Model (MM5), NOGAPS, and UKMET. The forecast phase diagrams are easily produced by directly using the model forecast isobaric height field. Since the explicit height field is used, no adjustments are made for known model biases with respect to cyclone development. These diagrams aid the structural evaluation of cyclones forecast by operational and research numerical models.

It was found during the 2001 hurricane season that the phase diagrams were useful in forecasting the subtropical-to-tropical conversion of (future) Hurricanes Karen and Olga (P. Bowyer 2001, personal communication). Further, the evolution and timing of extratropical transition for Hurricanes Gabrielle and Michelle in the 2001 season were well diagnosed and forecast by the phase diagrams provided in real time on the Web site. These diagrams aided the public and marine forecasts of cyclone evolution during this hurricane season (P. Bowyer 2001, personal communication and CMC official advisories; M. Lawrence and J. Beven 2001, personal communication and official NHC advisories; not shown). Based upon the success during the 2001 season, it is recommended that the many examples of phase transition (both tropical and extratropical) during the 2001 hurricane season (see <http://eyewall.met.psu.edu/cyclonephase>) should be used as schematics for anticipating similar phase transitions in the future.

The ability to compare several models' phase evolution for a given cyclone is also available on the Web site, giving the user the ability to estimate the predictability of the cyclone evolution (assuming that each model forecast has similar weight). For many cyclones, several models agree upon the forecast evolution (example shown in Fig. 14). This example is from an intensifying extratropical cyclone over cen-

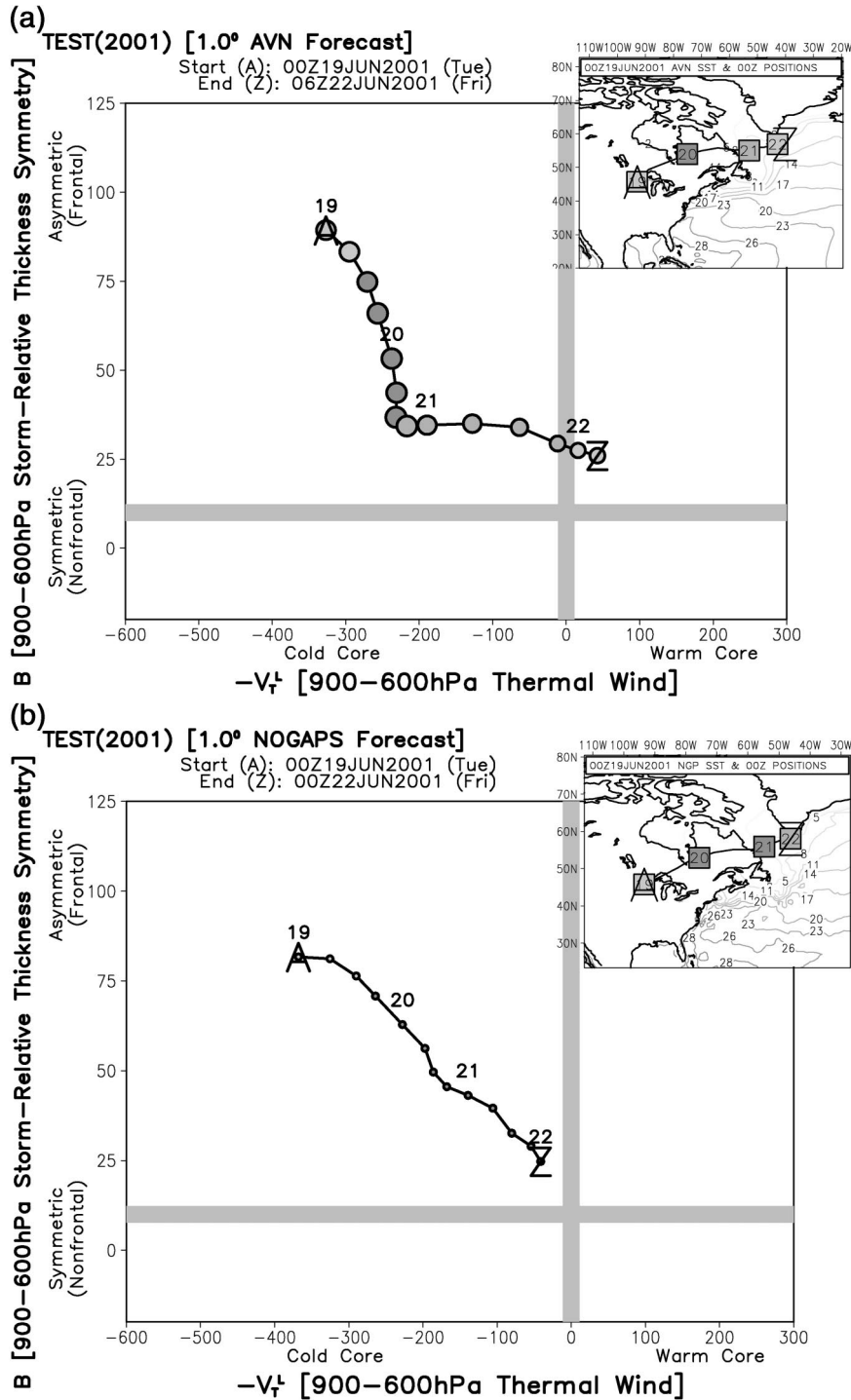


FIG. 14. Example application of the phase diagram in a forecast setting where there is considerable intermodel forecast agreement. (a) NCEP AVN, (b) NOGAPS, (c) UKMET, and (d) model consensus (mean) 72-h forecast initialized at 0000 UTC 19 Jun 2001 for an extratropical cyclone over central North America. Although there is variance among the models in the details of phase evolution [note one-standard deviation shading about the mean in (d)], all three models forecast the intensification and wind field expansion of the cyclone during the first 48 h of the forecast, followed by a weakening of the cold-core baroclinic structure, with the potential warm-core development late in the forecast (22 Jun 2001) for two of four models (AVN and NOGAPS).

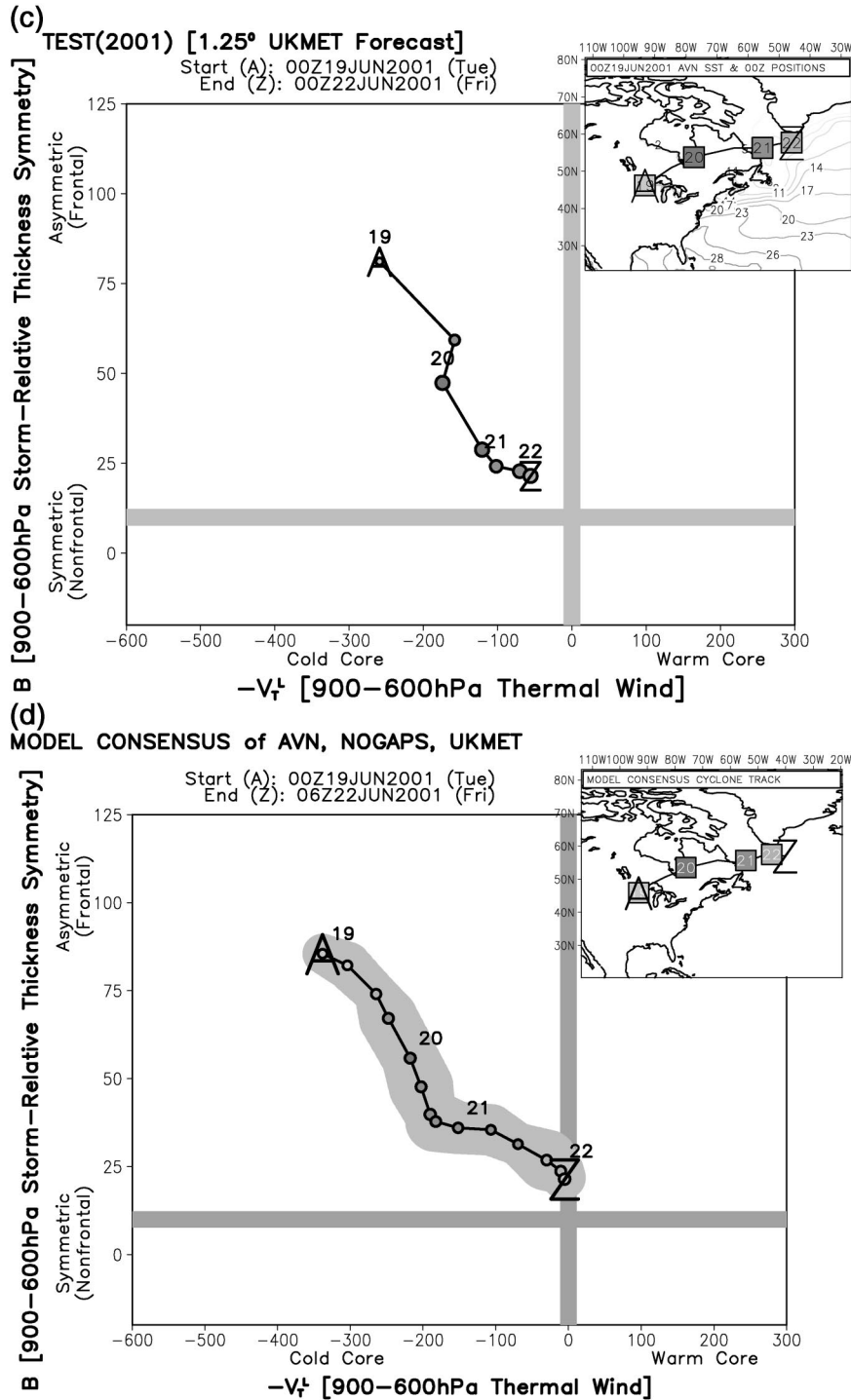


FIG. 14. (Continued)

tral North America in June 2001. All three models forecast a cold-core intensification of the cyclone, followed by a weakening of the cold-core structure. One of the three models forecast the cyclone to evolve into a warm-core system as it approaches southern Greenland, with the other two models stopping just short

of warm-core development. While the models generally agree on the broad evolution of the cyclone, they do disagree on the details of that evolution. The AVN and UKMET forecast a steadily weakening asymmetric structure, followed by weakening of the cold core, in two separate stages of cyclone evolution.

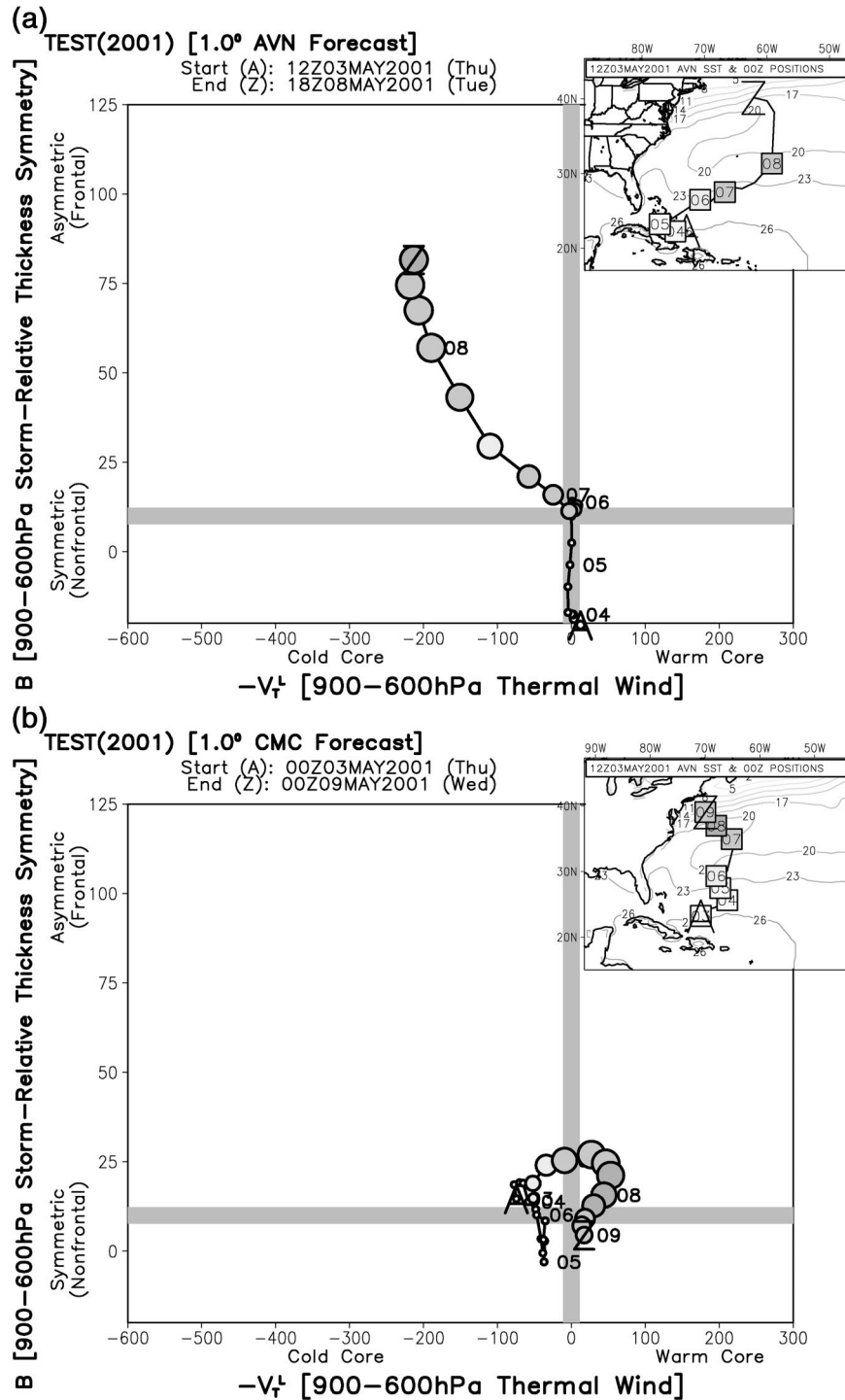


FIG. 15. Example application of the phase diagram in a forecast setting where there is significant intermodel forecast disagreement. (a) NCEP AVN, (b) CMC, (c) NOGAPS, and (d) model consensus (mean) 5-day forecast initialized on 3 May 2001 for the conversion of a weakly cold-core subtropical cyclone into (a) a marginal warm-core cyclone then a strong extratropical storm, (b) a strong hybrid cyclone, or (c) a weak hybrid cyclone. The shading about the mean in (d) illustrates that the phase forecast uncertainty grows with time, dominating the consensus mean forecast on 7 and 8 May. Real-time phase diagrams of analyzed and forecast cyclones are available at <http://eyewall.met.pou.edu/cyclonephase>.

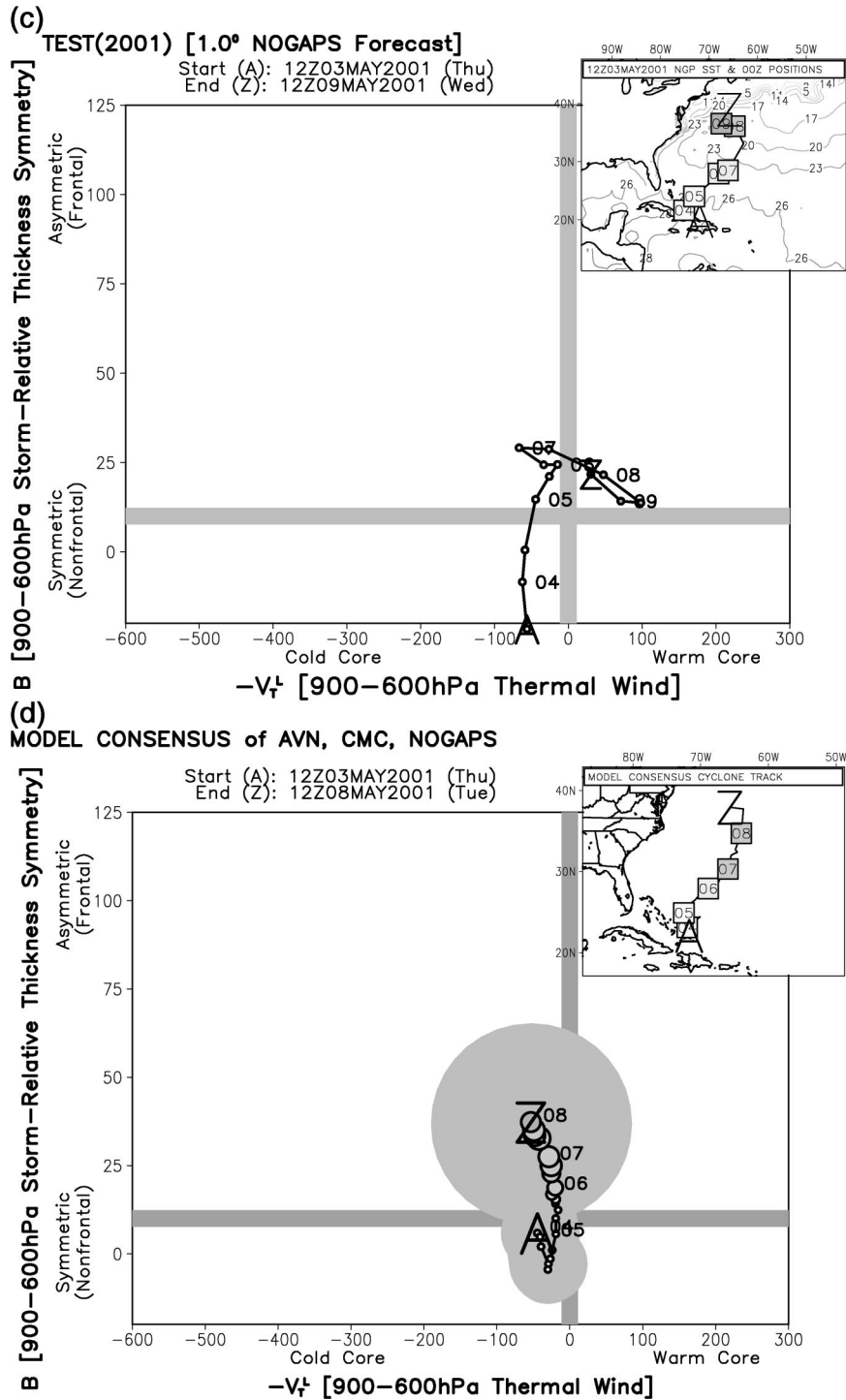


FIG. 15. (Continued)

In contrast, the NOGAPS forecast has a simultaneous decrease of both asymmetry and cold-core structure, giving diagonal movement with the diagram. The consensus track, intensity, and phase forecast are given in Fig. 14d, with the gray shading measuring the one

standard deviation variability among the models. It is expected for the range of model resolution and initialization methods that a model-to-model variability of approximately 10 for B and 25 for $-V_T^L$ and $-V_T^U$ is normal. Thus, despite these differences, this

example represents a case of impressive agreement among the forecast cyclone phase.

In contrast, many cyclones have a forecast evolution that is not agreed upon by the existing numerical models. Such an example is shown in Fig. 15, for the evolution of a weak subtropical cyclone north of Puerto Rico in early May 2001. The AVN forecasts a weak cold-core cyclone to develop marginal warm-core structure ($B \approx 10$, $-V_r^2 \approx +10$) through 6 May with slight intensification through that time. Beyond 6 May, the AVN forecasts intensification of the cyclone into a relatively strong cold-core extratropical cyclone (990 hPa at the end of the forecast). In contrast, both the CMC and NOGAPS forecast strikingly different phases despite similar tracks. The CMC forecasts intensification of the cold-core cyclone through 7 May, and then conversion of the cyclone into a moderately strong warm-core frontal cyclone (990 hPa on 8 May), before occluding as a nonfrontal warm-core cyclone at the end of the forecast period. Consistent with the forecast phase evolution, the AVN predicts an expanding wind field throughout the life cycle while the CMC forecasts an initial expansion associated with the cold-core development, followed by a contraction of the wind field as the warm-core evolution takes place. NOGAPS forecasts an evolution similar to the CMC model, although it produces a stronger warm core that remains at least marginally frontal through the end of the forecast. All three models forecast a similar maximum intensity for the cyclone, but do so through strikingly different trajectories through phase space. The gray shading within the consensus forecast in Fig. 14d indicates that beyond May 5, the cyclone may be warm or cold core, and weakly frontal or highly frontal, depending on the model of choice. There should be low confidence in the phase forecasts for this cyclone, unless a phase bias can be documented for certain members of the model ensemble in Fig. 15. Quantifying these model cyclone phase biases is anticipated for future extensions of this research.

Through routine evaluation of the phase diagrams forecast by operational models, estimation of cyclone phase predictability, of the potential sources for (forecasted or unforecasted) intensification based on forecast phase, and of potential track error evaluation is possible. A cyclone that is reliably predicted to transition to a warm-core structure may be expected to have greater potential intensity forecast errors than one that remains cold core, for example. Using the diagrams proposed here, this greater potential threat and forecast uncertainty can be anticipated if the consensus phase forecast indicates a warm-core evolution that may not be apparent from conventional analyses or forecasts of MSLP, equivalent potential temperature, surface wind fields, or precipitation.

7. Concluding summary

An objectively defined continuum for evaluating cyclone phase has been proposed and explored. Any cy-

clone with a closed surface circulation and well-resolved three-dimensional height field can be evaluated within the phase diagram using measures of lower-tropospheric thickness asymmetry (frontal nature) and tropospheric thermal wind (cold- versus warm-core structure) evaluated at two layers of equal depth. Conventional life cycles for tropical and extratropical cyclones are well represented within the phase diagram, using previously well-studied cases. Transitions between cold- and warm-core structure can be objectively identified, including extratropical transition, tropical transition, warm seclusions, and the development of hybrid cyclones, all of which are summarized in Fig. 16. Substantial insight into the structural changes during cyclone development at various phases within its life cycle can be evaluated based upon the location and movement within the diagram.

After examination of over 17 000 cyclones between 1980 and 1999, it is clear that natural boundaries between cyclone phases do not exist. Evolution of tropical cyclones into extratropical cyclones is a common occurrence and well diagnosed within the phase diagram. Evolution of warm-core structure within extratropical cyclones (warm seclusion) is another frequent life cycle that is resolved by the phase space. The conventional life cycle definitions for pure extratropical and tropical cyclones apply to a significant, but not overwhelming, percentage of the full continuum of cyclones. A significant percentage (est. 10%–15%; Fig. 13) of cyclones have both cold-core and warm-core phases of their life cycles. At 2.5° grid resolution, the development of a warm core is associated with an observed lower intensity bound that is 14 hPa stronger than a cyclone that remains cold core, suggesting an observed lower bound for cold-core cyclone structure that should be further refined using a longer dataset and at higher resolution.

Phase diagrams for current analyzed cyclones and operational model-forecast cyclones are available on the World Wide Web. This allows users to examine and anticipate the life cycle evolution of cyclones. More accurate diagnosis and forecasting of tropical transition, extratropical transition, and other cyclone phase transitions was shown during the 2001 hurricane season and will continue to be possible. Future research will examine the skill of the cyclone phase approach in anticipating tropical cyclone development and tropical cyclone transition. Further, consistency in forecast evolution between a number of models may provide insights into the predictability of the system as well as its structure and limits on its intensity. Additional future research will examine predictability within the phase space and a detailed examination of the synoptic evolution associated with the most common trajectories throughout the phase space presented here. After several months to years of phase analysis, model climatology of cyclone phase will be contrasted to understand the intrinsic biases in various cyclone developments that are associated with each model. Such biases will not only

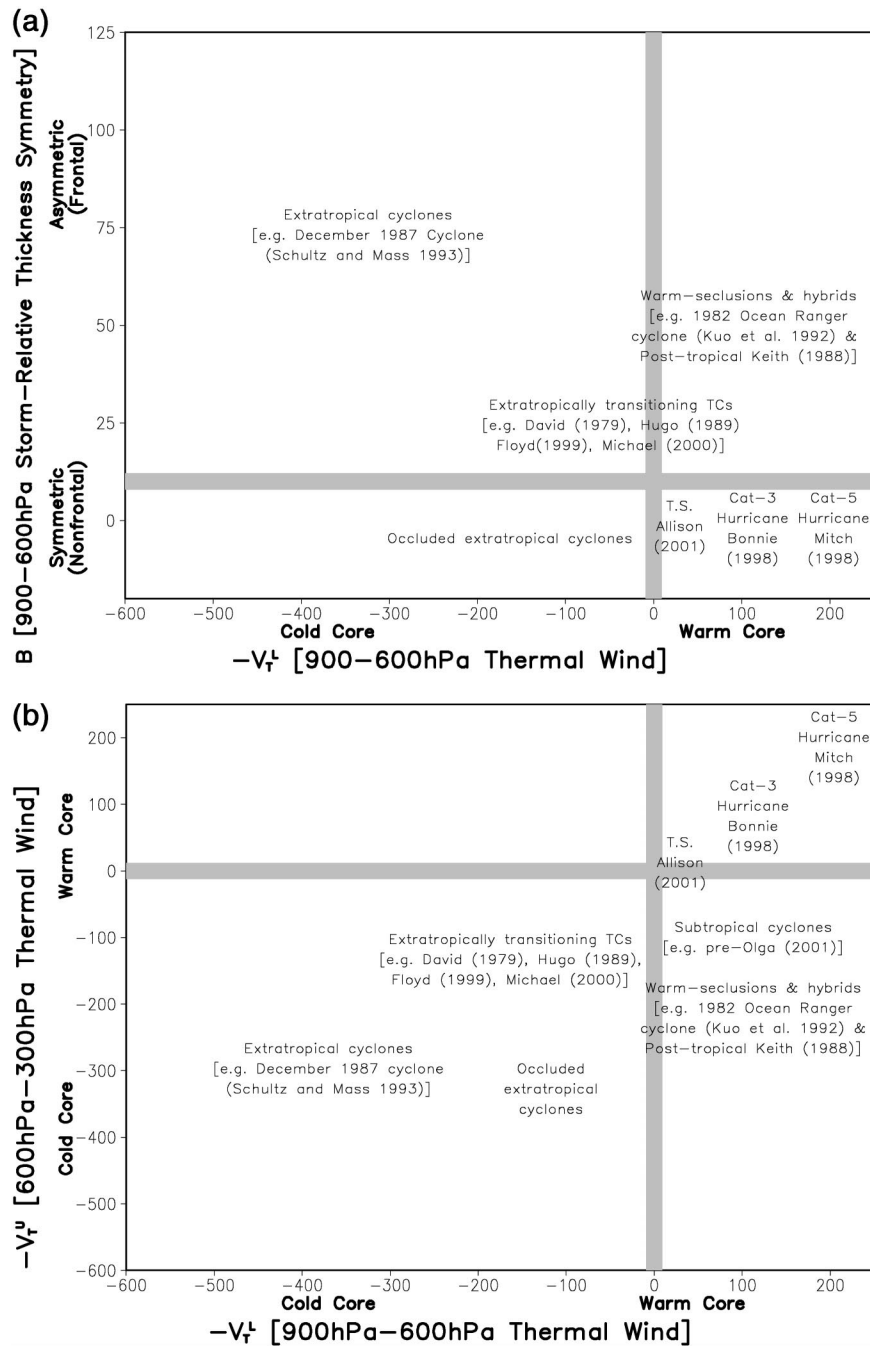


FIG. 16. Summary of the general locations of various cyclone types within the proposed phase space: (a) $-V_T^L$ vs B and (b) $-V_T^L$ vs $-V_T^U$. While cyclones may move throughout the phase space during their evolution, the plotted location is that most representative or unique of the cyclone type.

illuminate model weakness in cyclone analysis and forecasts, but provide for more accurate estimates of predictability and forecast uncertainty. The impact of bogus vortices in initial conditions on the phase space evolution should be examined. Further, the phase space may have utility in determining when bogusing should be ceased during extratropical transition, or when bogusing

should commence during tropical or subtropical transition.

Acknowledgments. Partial support for this research came from the National Science Foundation (ATM-9911212) and NASA (NAG5-7547). The author was funded by a Pennsylvania State University Earth-System

Science Center fellowship, an Environmental Protection Agency (EPA) STAR Graduate fellowship, and a NASA Space Grant Graduate fellowship. The author sincerely appreciates the support provided by these agencies.

The NOGAPS analysis and forecast data were provided by Mike Fiorino of Lawrence Livermore National Lab. The author is grateful to the Canadian Meteorological Center, the National Centers for Environmental Prediction (NCEP), and the U.K. Met Office (UKMET) for providing real-time gridded analysis and forecast data via the Internet. The availability of these real-time data sources was crucial to the application and implementation of this research for the operational and research forecast community through the URL provided in section 2b.

Figures for this paper and real-time analyses on the associated Web site were created using the GrADS software package from COLA/IGES. Sincere gratitude is given to the folks at COLA/IGES, including Brian Doty and Mike Fiorino (of LLNL) for making this software package available.

The author sincerely thanks Jenni Evans of The Pennsylvania State University for her critical and creative support, and whose comments on the manuscript have led to significant improvements. This research was greatly benefited by memorable discussions with and critical feedback from Jenni Evans, Barbara Prater, George Tsakraklides, Mike Fritsch, Nelson Seaman, Bill Frank, Todd Miner, Brian Etherton, Joby Hilliker, and George Bryan of Penn State; John Molinari and Lance Bosart of the University at Albany; Chris Velden of the University of Wisconsin; Jack Beven, Richard Pasch, and Miles Lawrence of the National Hurricane Center; and Pete Bowyer of the Canadian Hurricane Center. The author is grateful to Pat Harr of NRL for providing insight and references on cyclone tracking at NRL.

Critical reviews of the manuscript by Jack Beven, Lance Bosart, John Gyakum, and three anonymous reviewers are sincerely appreciated. In particular, an anonymous reviewer suggested the directional restriction for improving cyclone tracking.

REFERENCES

- Beven, J. L., II, 1997: A study of three "hybrid" storms. Preprints, *22d Conf. on Hurricanes and Tropical Meteorology*, Fort Collins, CO, Amer. Meteor. Soc., 645–646.
- Bister, M., and K. A. Emanuel, 1998: Dissipative heating and hurricane intensity. *Meteor. Atmos. Phys.*, **65**, 233–240.
- Bjerknes, J., and H. Solberg, 1922: Life cycle of cyclones and the polar front theory of atmospheric circulation. *Geophys. Publ.*, **3**, 1–18.
- Bosart, L. F., 1981: The Presidents' Day snowstorm of 18–19 February 1979: A subsynoptic-scale event. *Mon. Wea. Rev.*, **109**, 1542–1566.
- , and J. A. Bartlo, 1991: Tropical storm formation in a baroclinic environment. *Mon. Wea. Rev.*, **119**, 1979–2013.
- , and G. M. Lackmann, 1995: Postlandfall tropical cyclone reintensification in a weakly baroclinic environment: A case study of Hurricane David (September 1979). *Mon. Wea. Rev.*, **123**, 3268–3291.
- Brand, S., and C. P. Guard, 1978: Extratropical storm evolution from tropical cyclones in the western North Pacific Ocean. Naval Environmental Prediction Tech. Rep. TR 78-02, 20 pp.
- Brueske, K. F., and C. S. Velden, 2000: Tropical cyclone intensity estimation using the NOAA–KLM series Advanced Microwave Sounding Unit (AMSU): Preliminary results and future prospects. Preprints, *24th Conf. on Hurricanes and Tropical Meteorology*, Fort Lauderdale, FL, Amer. Meteor. Soc., 258–259.
- Caplan, P., J. Derber, W. Gemmill, S.-Y. Hong, H.-L. Pan, and D. Parrish, 1997: Changes to the 1995 NCEP operational Medium-Range Forecast model analysis–forecast system. *Wea. Forecasting*, **12**, 581–594.
- Charney, J. G., 1947: The dynamics of long waves in a baroclinic westerly current. *J. Meteor.*, **4**, 135–162.
- , and A. Eliassen, 1964: On the growth of the hurricane depression. *J. Atmos. Sci.*, **21**, 68–75.
- Côté, J., M. Roch, A. Staniforth, and L. Fillion, 1993: A variable-resolution semi-Lagrangian finite-element global model of the shallow-water equations. *Mon. Wea. Rev.*, **121**, 231–243.
- , J. G. Desmarais, S. Gravel, A. Méthot, A. Patoine, M. Roch, and A. Staniforth, 1998a: The operational CMC–MRB Global Environmental Multiscale (GEM) model. Part II: Results. *Mon. Wea. Rev.*, **126**, 1397–1418.
- , S. Gravel, A. Méthot, A. Patoine, M. Roch, and A. Staniforth, 1998b: The operational CMC–MRB Global Environmental Multiscale (GEM) model. Part I: Design considerations and formulation. *Mon. Wea. Rev.*, **126**, 1373–1395.
- Cullen, M. J. P., 1993: The Unified Forecast/Climate Model. *Meteor. Mag.*, **122**, 81–94.
- DiMego, G. J., and L. F. Bosart, 1982a: The transformation of Tropical Storm Agnes into an extratropical cyclone. Part I: The observed fields and vertical motion computations. *Mon. Wea. Rev.*, **110**, 385–411.
- , and —, 1982b: The transformation of Tropical Storm Agnes into an extratropical cyclone. Part II: Moisture, vorticity, and kinetic energy budgets. *Mon. Wea. Rev.*, **110**, 412–433.
- Dvorak, V. F., 1984: Tropical cyclone intensity analysis using satellite data. NOAA Tech. Rep. NESDIS 11, National Oceanic and Atmospheric Administration, Washington, DC, 47pp. [Available from National Technical Information Service, 5285 Port Royal Rd., Springfield, VA 22161.]
- Eady, E. T., 1949: Long waves and cyclone waves. *Tellus*, **1**, 33–52.
- Elsberry, R. L., Ed., 1995: *Global Perspectives on Tropical Cyclones*. WMO Rep. TD-No. 693, Geneva, Switzerland, 289 pp.
- Emanuel, K. A., 1986: An air–sea interaction theory for tropical cyclones. Part I: Steady state maintenance. *J. Atmos. Sci.*, **43**, 585–604.
- , 1988: The maximum intensity of hurricanes. *J. Atmos. Sci.*, **45**, 1143–1155.
- Evans, J. E., and R. Hart, 2003: Objective indicators of the life cycle evaluation of extratropical transition of Atlantic tropical cyclones. *Mon. Wea. Rev.*, in press.
- Frank, W. M., 1977: The structure and energetics of the tropical cyclone. I. Storm structure. *Mon. Wea. Rev.*, **105**, 1119–1135.
- Gibson, J. K., P. Kållberg, S. Uppala, A. Hernandez, A. Nomura, and E. Serrano, 1997: ERA description. ECMWF Re-analysis Project Report Series, No. 1, ECMWF, Shinfield Park, United Kingdom, 72 pp.
- Guiney, J. L., and M. B. Lawrence, 1999: Preliminary report: Hurricane Mitch. 22 October–05 November 1998. National Hurricane Center, 17 pp. [Available from Tropical Prediction Center, 11691 S.W. 17th Street, Miami, FL 33165-2149; also available online at <http://www.nhc.noaa.gov/1998mitch.html>.]
- Gyakum, J. R., 1983a: On the evolution of the *QE II* storm. Part I: Synoptic aspects. *Mon. Wea. Rev.*, **111**, 1137–1155.
- , 1983b: On the evolution of the *QE II* storm. Part II: Dynamic and thermodynamic structure. *Mon. Wea. Rev.*, **111**, 1156–1173.

- Hakim, G. J., L. F. Bosart, and D. Keyser, 1995: The Ohio Valley wave-merger cyclogenesis event of 25–26 January 1978. Part I: Multiscale case study. *Mon. Wea. Rev.*, **123**, 2663–2692.
- , D. Keyser, and L. F. Bosart, 1996: The Ohio Valley wave-merger cyclogenesis event of 25–26 January 1978. Part II: Diagnosis using quasigeostrophic potential vorticity inversion. *Mon. Wea. Rev.*, **124**, 2176–2205.
- Harr, P., and R. L. Elsberry, 2000: Extratropical transition of tropical cyclones over the western North Pacific. Part I: Evolution of structural characteristics during the transition process. *Mon. Wea. Rev.*, **128**, 2613–2633.
- , T. L. Tsui, and L. R. Brody, 1983: Model verification statistics tailored for the field forecaster. Preprints, *Eighth Conf. on Probability and Statistics in the Atmospheric Sciences*, Hot Springs, AR, Amer. Meteor. Soc., 177–180.
- , R. L. Elsberry, T. F. Hogan, and W. M. Clune, 1992: Forecasts of North Pacific maritime cyclones with the Navy Operational Global Atmospheric Prediction System. *Wea. Forecasting*, **7**, 456–467.
- , R. L. Elsberry, and T. Hogan, 2000: Extratropical transition of tropical cyclones over the western North Pacific. Part II: The impact of midlatitude circulation characteristics. *Mon. Wea. Rev.*, **128**, 2634–2653.
- Hart, R. E., 2001: The extratropical transition of Atlantic tropical cyclones: Climatology, lifecycle definition, and a case study. Ph.D. thesis, The Pennsylvania State University, 176 pp. [Available from The Pennsylvania State University, 503 Walker Bldg., University Park, PA 16802.]
- , and J. L. Evans, 2001: A climatology of the extratropical transition of Atlantic tropical cyclones. *J. Climate*, **14**, 546–564.
- Hebert, P. J., and K. O. Poteat, 1975: A satellite classification technique for subtropical cyclones. NOAA Tech. Memo. NWS SR-83, National Weather Service, 25 pp. [Available from NTIS, 5285 Port Royal Rd., Springfield, VA 22161.]
- Hirschberg, P. A., and J. M. Fritsch, 1993: On understanding height tendency. *Mon. Wea. Rev.*, **121**, 2646–2661.
- Hogan, T., and T. Rosmond, 1991: The description of the Navy Operational Global Atmospheric Prediction System's spectral forecast model. *Mon. Wea. Rev.*, **119**, 1786–1815.
- Jarvinen, B. R., C. J. Neumann, and M. A. S. Davis, 1984: A tropical cyclone data tape for the North Atlantic basin, 1886–1983: Contents, limitations, and uses. NOAA Tech. Memo. NWS NHC 22, 21 pp.
- Kalnay, E., and Coauthors, 1996: The NCEP/NCAR 40-Year Reanalysis Project. *Bull. Amer. Meteor. Soc.*, **77**, 437–471.
- Kanamitsu, M., 1989: Description of the NMC global data assimilation and forecast system. *Wea. Forecasting*, **4**, 335–342.
- Kidder, S. Q., M. D. Goldberg, R. M. Zehr, M. DeMaria, J. F. W. Purden, C. S. Velden, C. C. Goody, and S. J. Kusselson, 2000: Satellite analysis of tropical cyclones using the Advanced Microwave Sounding Unit (AMSU). *Bull. Amer. Meteor. Soc.*, **81**, 1241–1260.
- Klein, P., P. Harr, and R. L. Elsberry, 2000: Extratropical transition of western North Pacific tropical cyclones: An overview and conceptual model of the transformation stage. *Wea. Forecasting*, **15**, 373–396.
- Knox, J. L., 1955: The Storm "Hazel," synoptic resume of its development as it approached southern Ontario. *Bull. Amer. Meteor. Soc.*, **36**, 239–246.
- Kornegay, F. C., and D. G. Vincent, 1976: Kinetic energy budget analysis during interaction of Tropical Storm Candy (1968) with an extratropical frontal system. *Mon. Wea. Rev.*, **104**, 849–859.
- Kuo, J.-H., R. J. Reed, and S. Low-Nam, 1992: Thermal structure and airflow in a model simulation of an occluded marine cyclone. *Mon. Wea. Rev.*, **120**, 2280–2297.
- Lawrence, M. B., and L. A. Arila, J. L. Beren, J. L. Franklin, J. L. Guiney, and R. J. Pasch, 2001: Atlantic hurricane season of 1999. *Mon. Wea. Rev.*, **129**, 3057–3084.
- Marchok, T. P., 2002: How the NCEP tropical cyclone tracker works. Preprints, *25th Conf. on Hurricanes and Tropical Meteorology*, San Diego, CA, Amer. Meteor. Soc., 21–22.
- Mass, C. F., and D. M. Schultz, 1993: The structure and evolution of a simulated midlatitude cyclone over land. *Mon. Wea. Rev.*, **121**, 889–917.
- Miner, T., P. J. Sousounis, J. Wallman, and G. Mann, 2000: Hurricane Huron. *Bull. Amer. Meteor. Soc.*, **81**, 223–236.
- Neumann, C. J., B. R. Jarvinen, C. J. McAdie, and J. D. Elms, 1993: Tropical cyclones of the North Atlantic Ocean, 1871–1992. National Climatic Data Center in cooperation with the National Hurricane Center, Coral Gables, FL, 193 pp.
- Ooyama, K., 1969: Numerical simulation of the life-cycle of tropical cyclones. *J. Atmos. Sci.*, **26**, 3–40.
- Palmén, E., 1958: Vertical circulation and release of kinetic energy during the development of Hurricane Hazel into an extratropical storm. *Tellus*, **10**, 1–23.
- Petterssen, S., 1956: *Weather Analysis and Forecasting*. Vol. II. McGraw-Hill, 428 pp.
- Pierce, C. H., 1939: The meteorological history of the New England hurricane of Sept. 21, 1938. *Mon. Wea. Rev.*, **67**, 237–285.
- Reale, O., and R. Atlas, 2001: Tropical cyclone-like vortices in the extratropics: Observational evidence and synoptic analysis. *Wea. Forecasting*, **16**, 7–34.
- Reed, R. J., Y.-H. Kuo, and S. Low-Nam, 1994: An adiabatic simulation of the ERICA IOP4 storm: An example of quasi-ideal frontal cyclone development. *Mon. Wea. Rev.*, **122**, 2688–2708.
- Reynolds, R. W., and T. Smith, 1995: A high-resolution global sea surface temperature climatology. *J. Climate*, **8**, 1571–1583.
- Rotunno, R., and K. Emanuel, 1987: An air–sea interaction theory for tropical cyclones. Part II: Evolutionary study using a non-hydrostatic axisymmetric numerical model. *J. Atmos. Sci.*, **44**, 542–561.
- Sanders, F., 1987: Skill of NMC operational models in prediction of explosive cyclogenesis. *Wea. Forecasting*, **2**, 322–336.
- , and J. R. Gyakum, 1980: Synoptic–dynamic climatology of the "bomb." *Mon. Wea. Rev.*, **108**, 1589–1606.
- Schultz, D. M., and C. F. Mass, 1993: The occlusion process in a midlatitude cyclone over land. *Mon. Wea. Rev.*, **121**, 918–940.
- Sekioka, M., 1956a: A hypothesis on complex of tropical and extratropical cyclones for typhoon in the middle latitudes. I. Synoptic structure of Typhoon Marie passing over the Japan Sea. *J. Meteor. Soc. Japan*, **34**, 276–287.
- , 1956b: A hypothesis on complex of tropical and extratropical cyclones for typhoon in the middle latitudes. II. Synoptic structure of Typhoons Louise, Kezia, and Jane passing over the Japan Sea. *J. Meteor. Soc. Japan*, **34**, 336–345.
- , 1957: A hypothesis on complex of tropical and extratropical cyclones for typhoon in the middle latitudes. III. Examples of typhoon not accompanied by extratropical cyclone in the middle latitudes. *J. Meteor. Soc. Japan*, **35**, 170–173.
- Shapiro, L. J., and H. E. Willoughby, 1982: The response of balanced hurricanes to local sources of heat and momentum. *J. Atmos. Sci.*, **39**, 378–394.
- , and D. Keyser, 1990: Fronts, jet streams, and the tropopause. *Extratropical Cyclones: The Erik Palmén Memorial Volume*, C. W. Newton and E. O. Holopainen, Eds., Amer. Meteor. Soc., 167–191.
- Sinclair, M. R., 1994: An objective cyclone climatology for the Southern Hemisphere. *Mon. Wea. Rev.*, **122**, 2239–2256.
- Sutcliffe, R. C., 1947: A contribution to the problem of development. *Quart. J. Roy. Meteor. Soc.*, **73**, 370–383.
- Tannehill, I. R., 1938: Hurricane of September 16 to 22, 1938. *Mon. Wea. Rev.*, **66**, 286–288.
- Thorncroft, C., and S. C. Jones, 2000: The extratropical transitions of Hurricanes Felix and Iris in 1995. *Mon. Wea. Rev.*, **128**, 947–972.
- Trenberth, K. E., 1978: On the interpretation of the diagnostic quasigeostrophic omega equation. *Mon. Wea. Rev.*, **106**, 131–137.
- Velden, C. S., T. Olander, and S. Wanzong, 1998a: The impact of

- multispectral *GOES-8* wind information on Atlantic tropical cyclone track forecasts in 1995. Part I: Dataset methodology, description, and case analysis. *Mon. Wea. Rev.*, **126**, 1202–1218.
- , —, and R. M. Zehr, 1998b: Development of an objective scheme to estimate tropical cyclone intensity from digital geostationary satellite infrared imagery. *Wea. Forecasting*, **13**, 172–186.
- Williamson, D. L., 1981: Storm track representation and verification. *Tellus*, **33**, 513–530.
- Zishka, K. M., and P. J. Smith, 1980: The climatology of cyclones and anticyclones over North American and surrounding ocean environs for January and July, 1950–77. *Mon. Wea. Rev.*, **108**, 387–401.